Title
Activity-dependent FUS dysregulation disrupts synaptic homeostasis

Journal
Proceedings of the National Academy of Sciences of the United States of America, 111(44)

ISSN
0027-8424

Authors
Sephton, Chantelle F
Tang, Amy A
Kulkarni, Ashwinikumar
et al.

Publication Date
2014-11-04

DOI
10.1073/pnas.1406162111

Peer reviewed

Activity-dependent FUS dysregulation disrupts synaptic homeostasis

Chantelle F. Sephton[a,b,1], Amy A. Tang[c], Ashwinikumar Kulkarni[a,d], James West[a], Mieu Brooks[a], Jeremy J. Stubblefield[a], Yun Liu[a], Michael Q. Zhang[d,e], Carla B. Green[a], Kimberly M. Huber[a], Eric J. Huang[c], Joachim Herz[a,f], and Gang Yu[a,1]

Departments of [a]Neuroscience and [f]Molecular Genetics, University of Texas Southwestern Medical Center at Dallas, Dallas, TX 75390; [b]Institut Universitaire en Santé Mentale de Québec, Department of Psychiatry and Neuroscience, Université Laval, Quebec City, QC, Canada G1J 2G3; [c]Department of Pediatric Neuropathology and Developmental Neurobiology, University of California, San Francisco, CA 94143; [d]Department of Molecular and Cell Biology, University of Texas at Dallas, Richardson, TX 75080; and [e]Center for Synthetic and System Biology, Tsinghua National Laboratory of Information Science and Technology, Tsinghua University, Beijing 100084, China

Edited by Thomas C. Südhof, Stanford University School of Medicine, Stanford, CA, and approved September 17, 2014 (received for review April 2, 2014)

The RNA-binding protein fused-in-sarcoma (FUS) has been associated with amyotrophic lateral sclerosis (ALS) and frontotemporal lobar degeneration (FTLD), two neurodegenerative disorders that share similar clinical and pathological features. Both missense mutations and overexpression of wild-type FUS protein can be pathogenic in human patients. To study the molecular and cellular basis by which FUS mutations and overexpression cause disease, we generated novel transgenic mice globally expressing low levels of human wild-type protein (FUS^{WT}) and a pathological mutation (FUS^{R521G}). FUS^{WT} and FUS^{R521G} mice that develop severe motor deficits also show neuroinflammation, denervated neuromuscular junctions, and premature death, phenocopying the human diseases. A portion of FUS^{R521G} mice escape early lethality; these escapers have modest motor impairments and altered sociability, which correspond with a reduction of dendritic arbors and mature spines. Remarkably, only FUS^{R521G} mice show dendritic defects; FUS^{WT} mice do not. Activation of metabotropic glutamate receptors 1/5 in neocortical slices and isolated synaptoneurosomes increases endogenous mouse FUS and FUS^{WT} protein levels but decreases the FUS^{R521G} protein, providing a potential biochemical basis for the dendritic spine differences between FUS^{WT} and FUS^{R521G} mice.

FUS | frontotemporal lobar degeneration | amyotrophic lateral sclerosis | metabotropic glutamate receptors | synaptic homeostasis

Amyotrophic lateral sclerosis (ALS) is characterized by the degeneration of upper and lower motor neurons, leading to muscle weakness, paralysis, and death within 3–5 y of onset. Interestingly, ∼10–15% of ALS patients have clinical features of frontotemporal lobar degeneration (FTLD), marked by a decline in decision-making, behavioral control, emotion, and language, and as many as half have mild-to-moderate cognitive or behavioral abnormalities (1). FTLD comprises a group of heterogeneous diseases characterized by progressive neurodegeneration of the frontal and temporal lobes and clinically by frontotemporal dementia (FTD) with or without motor neuron disease. There is no cure or effective therapy for those who suffer from ALS or FTLD, and the mechanisms by which these diseases occur are not well understood.

The clinical, pathological, and genetic overlap between ALS and FTLD suggests that there are mechanisms shared by these diseases. The RNA-binding proteins fused in sarcoma (FUS) and transactive response DNA-binding protein-43 (TDP-43) are the major protein components of inclusions that are characteristic of ALS and FTLD-U (FTLD with ubiquitinated inclusions) (2). More than 50 genetic *FUS* mutations have been identified in these related neurodegenerative disorders (3). Similarly, more than 40 dominant mutations in the *TDP-43* gene have been linked to ALS cases and, to a lesser extent, to FTLD (4). The identification of mutations in the *FUS* and *TDP-43* genes has provided insights for uncovering the disease mechanisms for ALS and FTLD.

FUS is a ubiquitously expressed RNA-binding protein that exists in dynamic ribonucleoprotein complexes involved in pre-mRNA splicing, mRNA stability, and mRNA transport. FUS is a member of the FET family of proteins that bind RNAs (5) and contains an RNA recognition motif, three arginine-glycine-glycine (RGG) boxes, and a zinc finger (ZnF) (6). RGG2-ZnF-RGG3 is the major RNA-binding domain, which has a preference for GU-rich sequences (7, 8). The N terminus of FUS contains a low-complexity sequence domain involved in RNA granule formation (9). Nucleocytoplasmic shuttling of FUS occurs by a nonclassical proline-tyrosine nuclear localization signal (PY-NLS) and a nuclear export signal (NES) (10). Methylation of the C-terminal RGG3 domain of FUS is necessary for transportin 1 interaction and nuclear localization (11).

The majority of clinical ALS/FTLD-associated FUS mutations occur in its C-terminal PY-NLS sequence (12), which is believed to enhance the cytoplasmic localization and aggregation propensity of the protein and reduce its ability to bind nuclear RNAs. In response to various stressors, FUS localizes into cytoplasmic stress granules (13). In neurons, there is more immunodetectable FUS at dendritic spines in response to metabolic glutamate receptor (mGluR) agonists (14). Moreover, neurons cultured from

Significance

Both overexpression of wild-type fused in sarcoma (FUS) protein and missense mutations can be pathogenic in a group of related neurodegenerative disorders that includes amyotrophic lateral sclerosis and frontotemporal lobar degeneration. It is unclear how FUS overexpression and missense mutations cause disease in human patients. In this work, we generated novel transgenic mouse models expressing low levels of wild-type and mutant human FUS, both of which recapitulate aspects of the human diseases. We found a profound difference in the underlying mechanisms by which missense mutation and wild-type overexpression cause disease. Overexpression of wild-type FUS protein alters its nuclear function at the level of gene expression. In contrast, missense mutation disrupts activity-dependent synaptic homeostasis to gain a toxic function at dendritic spines.

Author contributions: C.F.S., E.J.H., and G.Y. designed research; C.F.S., A.A.T., A.K., J.W., M.B., and J.J.S. performed research; C.F.S., Y.L., M.Q.Z., C.B.G., K.M.H., E.J.H., J.H., and G.Y. contributed new reagents/analytic tools; C.F.S., A.A.T., A.K., J.W., M.B., J.J.S., Y.L., M.Q.Z., C.B.G., K.M.H., E.J.H., J.H., and G.Y. analyzed data; and C.F.S. and G.Y. wrote the paper.

The authors declare no conflict of interest.

This article is a PNAS Direct Submission.

Freely available online through the PNAS open access option.

[1]To whom correspondence may be addressed. Email: Chantelle.Sephton.1@ulaval.ca or Gang.Yu@UTSouthwestern.edu.

This article contains supporting information online at www.pnas.org/lookup/suppl/doi:10.1073/pnas.1406162111/-/DCSupplemental.

FUS-knockout mice have abnormal spine morphology and spine density (14). It is unclear whether pathological FUS mutations disrupt activity-dependent synaptic structure or function.

Besides missense mutations at the C terminus of FUS protein, overexpression of wild-type FUS caused by mutations in its 3′ UTR also has been linked to ALS (15), suggesting that overexpression of wild-type FUS is pathogenic under certain circumstances. Indeed, pathogenic effects of increased levels of wild-type proteins are common in other neurodegenerative disorders, as exemplified by increased gene dose or overexpression of wild-type TDP-43, α-synuclein, and amyloid β precursor protein (APP) in ALS/FTLD, Parkinson disease, and Alzheimer's disease (16–18). However, in all these cases (including FUS), it is unclear whether protein overexpression and missense mutations contribute to neurodegenerative disorders via common or distinct mechanisms. In this work, we developed novel FUS transgenic mice expressing low levels of human wild-type FUS (FUS^{WT}) and an ALS-associated missense mutation (FUS^{R521G}), which is located in the PY-NLS, to investigate the pathological consequences and molecular mechanisms of FUS overexpression and missense mutation.

Results

Development of Cre-Inducible Transgenic Mice Globally Overexpressing Low Levels of Human FUS^{WT} and FUS^{R521G}. We generated transgenic mice expressing human wild-type FUS or the R521G mutation under the control of the cytomegalovirus immediate early enhancer-chicken β-actin hybrid (CAG) promoter (Fig. 1*A*), referred to as "CAG-FUS^{WT}" and "CAG-FUS^{R521G}," respectively. In this study, we chose to overexpress the FUS transgenes globally, starting from germ line and at low levels to recapitulate more closely the expression profile and FUS levels in patients with ALS and FTLD, because FUS is ubiquitously expressed in human tissues, and human patients carry FUS mutations (or overexpressed wild-type protein) all their lives, starting from germ line. Accordingly, two mouse lines harboring *CAG-Z-FUS^{WT}-IRES-EGFP* or *CAG-Z-FUS^{R521G}-IRES-EGFP* were crossed with the germ-line Meox2Cre mice. Cre recombinase excises the *LacZ* DNA sequence flanked by loxP sequences, allowing translation of FUS and GFP (Fig. 1 *B* and *C*). Transgenic CAG-FUS^{WT} mice (lines 629 and 638) and CAG-FUS^{R521G} mice (lines 673 and 682) were born at normal Mendelian ratios (*SI Appendix*, Table S1). Analysis of total brain lysates from CAG-FUS^{WT} (line 638) and CAG-FUS^{R521G} (line 682) mice showed that the level of human FUS expression was similar to that of endogenous mouse FUS (Fig. 1*D*).

Mice from CAG-FUS^{WT} (629 and 638) and CAG-FUS^{R521G} (673 and 682) transgenic lines were found to have reduced lifespan (Fig. 1 *E* and *F*): Nearly 100% of CAG-FUS^{WT} (lines 629 and 638) mice die before postnatal day (P)30, and ∼70% of the CAG-FUS^{R521G} (line 673) and ∼50% of CAG-FUS^{R521G} (line 682) mice have early lethality before P30. In monitoring the body weights of these mice from birth, we observed that the body weights of CAG-FUS^{WT} mice are significantly different from their littermates starting at ∼P4 (Fig. 1*G* and *SI Appendix*, Fig. S2*A*). The weight differences between CAG-FUS^{R521G} mice and their littermates are less obvious (Fig. 1*H* and *SI Appendix*, Fig. S2*B*). CAG-FUS^{WT} mice developed gait abnormalities at P10. By P14 their grip strength and righting ability were reduced, and hindlimb clasping was present (Fig. 1 *I* and *J* and *SI Appendix*, Table S2). Animals at this stage either died or were euthanized. Compared with the CAG-FUS^{WT} mice, the CAG-FUS^{R521G} mice that die early display similar but less severe impairments in locomotion in terms of gait, grip strength, righting ability, and hindlimb clasping (Fig. 1 *K* and *L* and *SI Appendix*, Table S2). The CAG-FUS^{R521G} mice that escaped early lethality had somewhat reduced body mass and displayed subtle motor impairment (*SI Appendix*, Fig. S2 *C–E*).

Defective Neuromuscular Synapses and Neuroinflammation in Juvenile CAG-FUS^{WT} and CAG-FUS^{R521G} Mice with Severe Motor Impairment. Inflammation, degeneration of motor neurons, and FUS aggregation are present in patients with ALS-FUS (3, 19, 20). We examined brains and spinal cords of end-stage CAG-FUS^{WT} and CAG-FUS^{R521G} mice and found no detectible cytoplasmic FUS localization or protein aggregates (*SI Appendix*, Fig. S1 *E–H*). Using immunohistochemistry, we then examined the activation of microglia and astrocytes as markers for neuroinflammation in the brains and spinal cords of end-stage CAG-FUS^{WT} and CAG-FUS^{R521G} mice. We found evidence of activation of astrocytes and microglia in all regions of the brain and spinal cord (Fig. 2 *A* and *B* and *SI Appendix*, Fig. S3 *A* and *B*). In contrast, CAG-FUS^{R521G} mice that escaped early lethality did not have these markers of neuroinflammation (*SI Appendix*, Fig. S3 *C* and *D*).

ALS patients develop muscle atrophy caused by the degeneration of spinal motor neurons, together with axonal degeneration and sclerosis of the later columns of the spinal cord, which contain the corticospinal tracts. Examination of the lumbar region of the spinal cord revealed no degeneration of axons in the dorsal corticospinal tract or lateral columns or in the dorsal or ventral roots (*SI Appendix*, Fig. S4 *B* and *C*), indicating that descending motor axons were not altered in CAG-FUS^{WT} or CAG-FUS^{R521G} mice. Muscle histology from end-stage CAG-FUS^{WT} and CAG-FUS^{R521G} mice showed scattered and grouped atrophic muscle fibers (Fig. 2*C*), a characteristic of denervation in muscle from patients with ALS. CAG-FUS^{WT} muscle showed more severe abnormalities, as observed by the presence of pyknotic myofibers (Fig. 2*C*, *Left*), whereas muscle abnormalities in CAG-FUS^{R521G} mice were less severe (Fig. 2*C*, *Right*). Quantification of spinal motor neuron numbers in the cervical spinal cord of CAG-FUS^{WT} and CAG-FUS^{R521G} mice showed no evidence of neuron loss as compared with control littermates (Fig. 2 *D* and *E*). Importantly, there were abnormalities in the neuromuscular junctions (NMJs) of end-stage animals (*SI Appendix*, Fig. S5), and analysis of the NMJs revealed significant denervation (Fig. 2 *F–H*). Our results indicate that degeneration of NMJs and muscle atrophy contribute to loss of motor function in CAG-FUS^{WT} and CAG-FUS^{R521G} mice.

FUS has been implicated in transcriptional and posttranscriptional regulation of gene expression (21–26). We therefore asked whether changes in gene-expression patterns in CAG-FUS^{WT} and CAG-FUS^{R521G} mice explain both the similarities and differences in the behavioral and cellular phenotypes of the wild-type and mutant transgenic mice. To do so, we generated paired-end RNA sequencing (RNA-seq) libraries from total RNA isolated from spinal cords of CAG-FUS^{WT} and CAG-FUS^{R521G} mice and their littermate controls. To avoid secondary effects of end-stage mice on gene expression, we selected transgenic mice that had not yet shown severe deficits in motor function and did not meet our end-stage criteria. To this end, we used P20 mice with a health score between 1 and 2 (as described in *Materials and Methods*). We carefully selected these mice to be phenotypically similar. Additionally, the samples for each RNA-seq library ($n = 2$ for each genotype) were pooled from three individual mice, to take into account any phenotype variability (see *SI Appendix*, *Supplemental Experimental Procedures* for details). The analysis from CAG-FUS^{WT} mice revealed 185 differentially expressed genes (with adjusted P value <0.05) (*SI Appendix*, Fig. S6*A* and Table S3). Genes with increased expression are enriched with Gene Ontology (GO) terms related to immune response: "DNA replication, recombination and repair" and "regulation of cell proliferation." Genes with decreased expression show GO terms related to lipid and sterol biosynthesis. In contrast, CAG-FUS^{R521G} mice had very few genes that were differentially expressed (with adjusted P value <0.05) (*SI Appendix*, Fig. S6*B* and Table S3), yielding no significant GO terms. The transcriptome profiles of

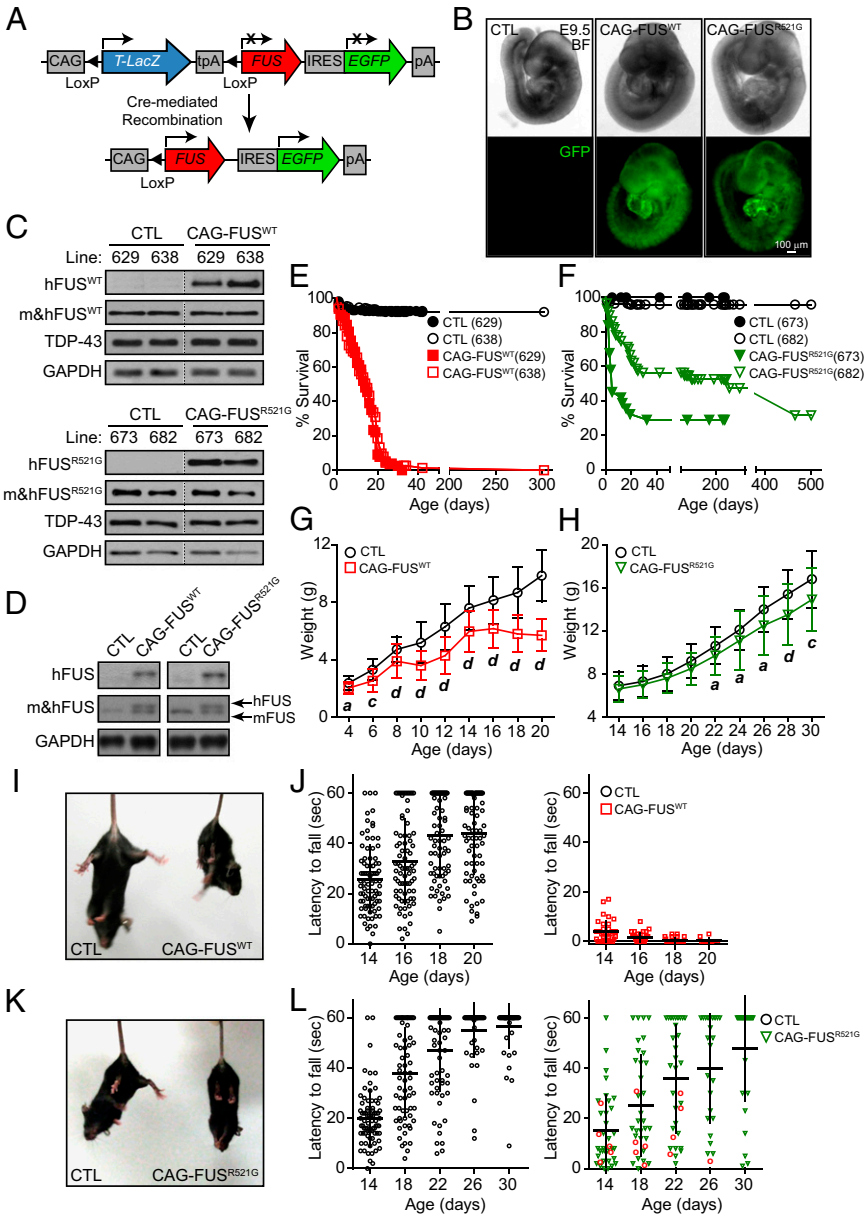

Fig. 1. Generation of CAG-FUS transgenic mice. (*A*) Schematic of the *CAG-Z-FUS-IRES-EGFP* transgenic construct. Mice carrying the *CAG-Z-FUS-IRES-EGFP* transgene are crossed with germ-line Meox2Cre mice. Cre recombinase excises the DNA sequence flanked by loxP sequences, allowing translation of FUS (red) and EGFP (green). (*B*) Embryos at E9.5 (bright field, BF) that have both *Meox2Cre* and *CAG-Z-FUS^{WT}-IRES-EGFP* (CAG-FUS^{WT}) or *CAG-Z-FUS^{R521G}-IRES-EGFP* (CAG-FUS^{R521G}) have global GFP expression. (*C*) Immunoblot of lysates from P0 mouse brains from CAG-FUS^{WT} (lines 629 and 638) and CAG-FUS^{R521G} (lines 673 and 682) transgenic lines for human (h)FUS, total mouse and human (m&h)FUS (shown is the FUS Santa Cruz antibody), TDP-43, and GAPDH. Samples were pooled from three pups from each line. (*D*) Immunoblot of P20 mouse whole brain showing hFUS and resolved endogenous mouse and exogenous (m&h)FUS proteins (shown is the FUS Sigma antibody) from CAG-FUS^{WT} (638) and CAG-FUS^{R521G} (682) mice. (*E* and *F*) Survival curves of CAG-FUS^{WT} (*E*) and CAG-FUS^{R521G} (*F*) mice. (*G* and *H*) Body weight curves of CAG-FUS^{WT} (638) (P4–P20) (*G*) and CAG-FUS^{R521G} (682) (P14-P30) (*H*) mice. (*I* and *K*) CAG-FUS^{WT} (*I*) and CAG-FUS^{R521G} (*K*) mice display hindlimb curl. (*J* and *L*) Grip test of CAG-FUS^{WT} mice (638), postnatal stages (P14–P20) (n = 21 litters) (*J*) and of CAG-FUS^{R521G} mice (682), postnatal stages (P14–P30) (n = 17 litters) (*L*). Red circles indicate CAG-FUS^{R521G} mice that had severe deficits in motor function and early lethality. Quantification is shown in *SI Appendix*, Table S2. (*G* and *H*) a, $P < 0.05$; b, $P < 0.01$; c, $P < 0.005$; d, $P < 0.001$ (one-way repeated measures ANOVA and post hoc Tukey test). Error bars represent SD of the mean.

these mice are consistent with the phenotypic differences observed between the CAG-FUS^{WT} and CAG-FUS^{R521G} transgenic models, wherein altering wild-type FUS levels is more deleterious than expression of FUS^{R521G}.

Impaired Motor Function and Sociability in Adult FUS^{R521G} Transgenic Mice. CAG-FUS^{R521G} mice that escape early lethality were monitored further. They showed persistently lower body weight (*SI Appendix*, Fig. S2 *C* and *D*) with no obvious deficits in locomotion (Fig. 3*D* and *SI Appendix*, Fig. S7*A*) and displayed subtle behavioral differences as compared with their littermates. The motor function of CAG-FUS^{R521G} mice was assessed on a rotorod over a 2-d period. On day 1 of rotorod testing, CAG-FUS^{R521G} mice performed as well as their littermate controls, but on day 2 they had impaired motor function (Fig. 3*A*). CAG-FUS^{R521G} mice were monitored on voluntary running wheels and showed less activity over a 9-d period (Fig. 3*B*). Despite the reduction in overall locomotor activity, food intake was not altered significantly (*SI Appendix*, Fig. S7 *B* and *C*). Gait analysis of the CAG-FUS^{R521G} mice revealed that the braking phase was greater in the forelimbs (Fig. 3*C* and *SI Appendix*, Table S4), and the swing phase was reduced in the hindlimbs (Fig. 3*C* and *SI Appendix*, Table S5). Results from the ladder-walking test indicate that the forelimbs have more errors in stepping with few deficits in the hindlimbs (*SI Appendix*, Fig. S7 *E–H*). These data indicate that deficits in the motor function of the CAG-FUS^{R521G} mice are modest and are more prominent when their motor function is challenged.

We also examined the social interactions of CAG-FUS^{R521G} mice with intruder/novel juvenile and adult mice. We found that the interaction with juvenile mice was significantly reduced at 4 mo of age (*SI Appendix*, Fig. S7*I*). When introduced to intruder adult mice, CAG-FUS^{R521G} mice did not show any significant deficits before 8 mo of age (Fig. 3*E* and Movies S1 and S2). We analyzed the types of social interactions of 8-mo-old CAG-FUS^{R521G} mice with an intruder adult and found that chasing behavior was reduced in CAG-FUS^{R521G} mice (Fig. 3*F*). No alterations in cognitive function or olfaction were detected in the CAG-FUS^{R521G} mice (*SI Appendix*, Fig. S7 *J* and *K*).

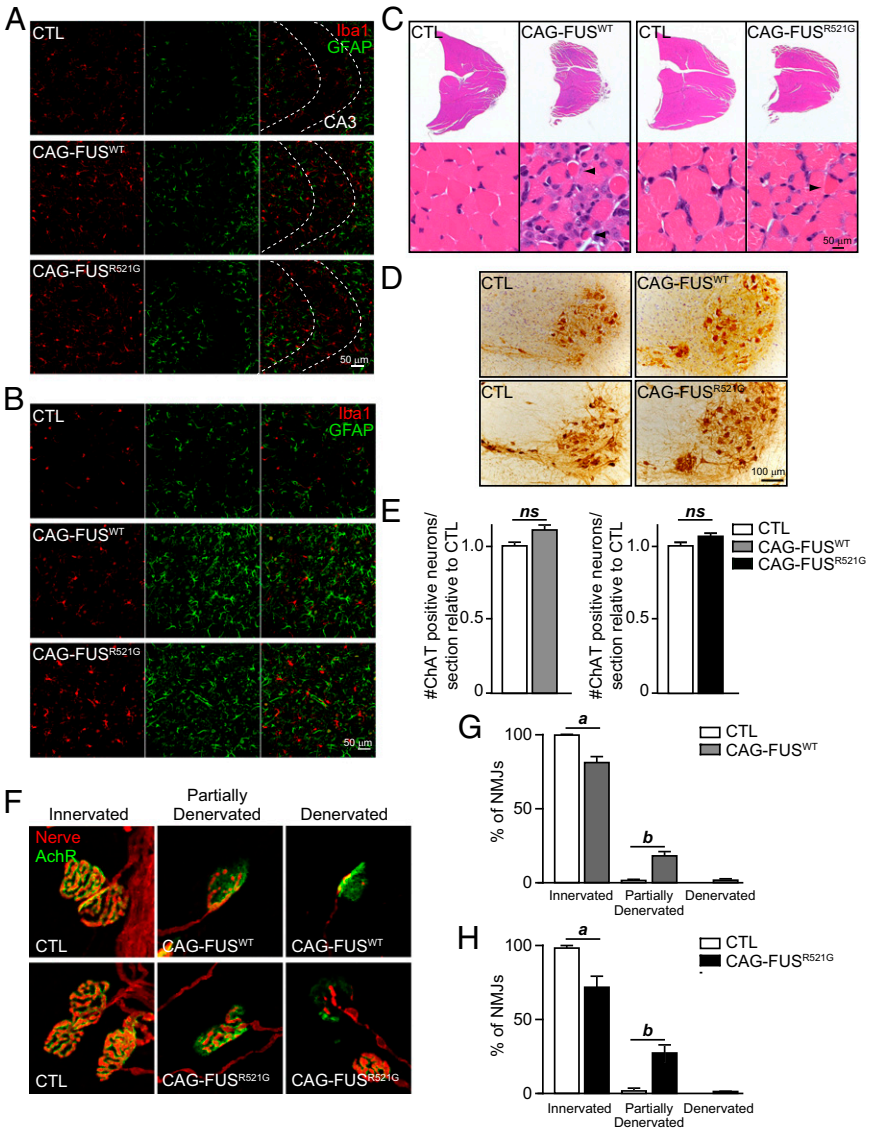

Fig. 2. Gliosis, muscle atrophy, and denervated NMJs in CAG-FUS^{WT} and CAG-FUS^{R521G} mice. (*A* and *B*) Immunofluorescence staining of the CA3 region of the hippocampus (*A*) and of the ventral horn of the spinal cord (*B*) for Iba1 (microglia; red) and GFAP (astrocytes; green) of end-stage mice. Images are representative of three animals per genotype. (*C*) H&E staining of the gastrocnemius muscle of CAG-FUS^{WT} and CAG-FUS^{R521G} mice at end stage show wasting of the muscle and scattered and grouped muscle atrophy, characteristic of motor axon degeneration. Arrowheads indicate pyknotic myofibers. Images are representative of three animals per genotype. (*D*) Immunostaining for ChAT highlights motor neurons in the cervical spinal cord of CAG-FUS^{WT} and CAG-FUS^{R521G} mice. (*E*) Quantification of spinal motor neuron numbers in the cervical spinal cord of CAG-FUS^{WT} and CAG-FUS^{R521G} mice show no evidence of neuron loss compared with control littermates. $n = 3$ CAG-FUS^{WT} mice and littermate controls, and $n = 4$ CAG-FUS^{R521G} mice and littermate controls. ns, not significant (Student *t* test). (*F*) Costaining for presynaptic terminals (nerve; red) and with bungarotoxin for postsynaptic terminals (AchR; green) shows that NMJs are denervated in P20–P24 CAG-FUS^{WT} and CAG-FUS^{R521G} mice at end stage compared with littermate controls. (*G* and *H*) Quantification of innervated NMJs. a, $P < 0.05$; b, $P < 0.01$ (Student *t* test). Error bars represent SD of the mean.

Altered Dendritic Branching in Spinal Motor Neurons and Sensorimotor Neurons of CAG-FUS^{R521G} Mice. FUS is found in RNA granules at dendritic spines, and immunodetectable FUS at synapses increases in response to group 1 mGluR stimulation (14, 27). Hippocampal cultures from FUS-knockout mice have altered dendritic branching and reduced mature spines (14), suggesting that FUS has an important role at the synapse. We hypothesized that deficits in motor function and sociability in the CAG-FUS^{R521G} "escapers" could be caused by alterations in dendrites or dendritic spines in the motor neurons and/or sensory motor cortex. We first examined the dendrites of spinal motor neurons in P18 FUS transgenic mice and found no reduction in the number of dendritic intersections or cumulative area in CAG-FUS^{WT} mice (Fig. 4 *A* and *D*). In contrast, the dendritic intersections and cumulative area of dendrites were reduced significantly in spinal motor neurons in CAG-FUS^{R521G} mice of the same age (Fig. 4 *B* and *D*). We then examined the CAG-FUS^{R521G} escapers at age 2 mo (P60). Even though the distribution of the numbers of intersections and cumulative area of dendrites were slightly different in P18 and P60 mice, we found significant and persistent deficits in the dendritic branches in spinal motor neurons (Fig. 4 *C* and *D*). Moreover, analysis of apical and basal dendrites in neurons in sensorimotor cortex layers IV–V in CAG-FUS^{R521G} mice showed fewer intersections and reduced cumulative area in the apical and basal dendrites of P18 and P60 mice (Fig. 4 *E* and *F*).

Activity-Dependent Reduction of FUS^{R521G} Protein Levels at Synapses. Cultured neurons from FUS-knockout mice have abnormal spine morphology as well as spine density (14). Therefore we decided to examine whether our transgenic models had alterations in the number of mature spines. We found that there was no difference in the total number of mature spines in the CAG-FUS^{WT} mice, but CAG-FUS^{R521G} mice had a significant decrease in the number and density of mature spines (Fig. 5 *A* and *B*).

Activation of group 1 mGluRs in hippocampal neurons has been shown to affect spine shape in a protein synthesis-dependent manner (28). Given what is known about the existence of FUS at synapses and its response to mGluR signaling, we hypothesized that deficits in dendritic branching and spine formation may stem from altered responses of FUS^{R521G} protein to mGluR activation. To test this hypothesis, we determined whether FUS^{R521G} protein displayed an altered synaptic expression upon activation of mGluRs. Using acute cortical tissue slices, we demonstrated that endogenous mouse FUS and human FUS^{WT} protein levels are increased in total cell lysates and in synaptoneurosome fractions after treatment with the group 1 mGluR agonist

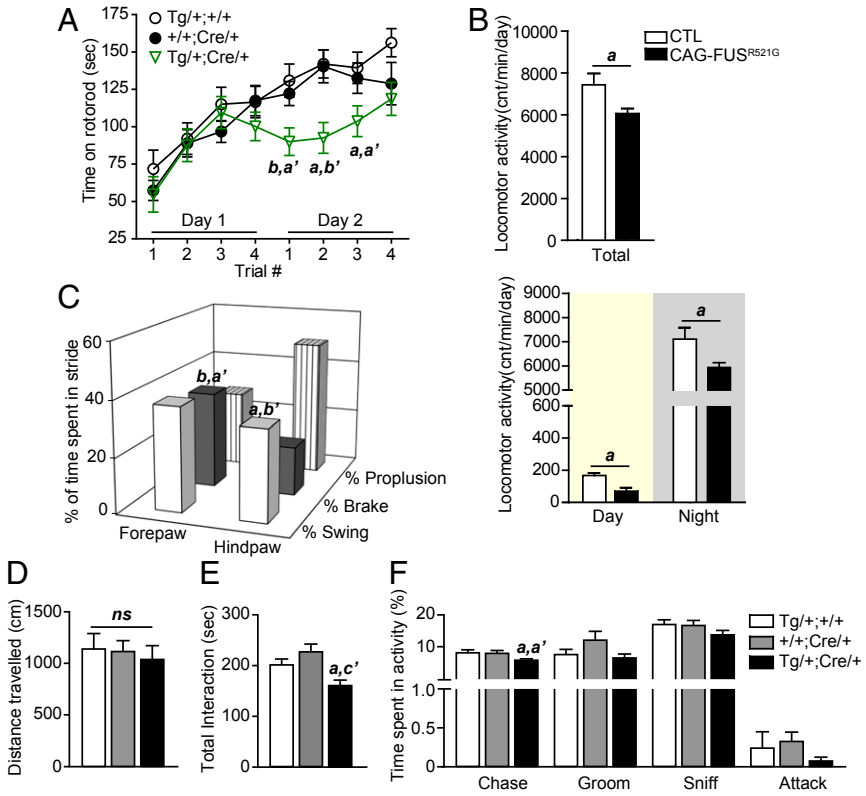

Fig. 3. Decline in motor function and social interaction in CAG-FUS^{R521G} transgenic mice that escape early lethality. (*A*) Rotorod performance of 2-mo-old CAG-FUS^{R521G} mice showing motor impairment on day 2. (*B*) Total running-wheel activity of 2-mo-old CAG-FUS^{R521G} mice (*Upper*) and their activity during the day and night (*Lower*). cnt, wheel revolutions. (*C*) Gait analysis of 2-mo-old CAG-FUS^{R521G} mice showing that the braking phase is greater in the forepaws and the swing phase is greater in the hindpaws. (*D*) Open field test in 8-mo-old mice shows no differences in total distance traveled. (*E* and *F*) The resident/intruder test in 8-mo-old CAG-FUS^{R521G} mice age shows significant reduction in total interactions (*E*) and particularly in chasing behavior (*F*). (*A*, *C*, and *D–F*) Three-way statistical comparisons with littermate controls used one-way ANOVA. a, $P < 0.05$; b, $P < 0.01$. (′ compares $^{+/+}$;Cre/+ with Tg/+;Cre/+). ns, not significant. (*B*) a, $P < 0.05$; b, $P < 0.01$; c, $P < 0.001$ (Student *t* test). Error bars represent SEM.

(R,S)-3,5-dihydroxyphenylglycine (DHPG) (Fig. 5 *C* and *D*). This result is consistent with an increase in immunodetectable FUS at synapses in response to mGluR stimulation previously reported in dissociated hippocampal cultured neurons (14, 27). In contrast, FUS^{R521G} protein levels were reduced in response to DHPG treatment in acute cortical slices (Fig. 5 *C* and *D*). These results indicate that mutant FUS does not respond properly to mGluR activation, and the reduced FUS levels may lead to the altered dendritic branching and spines.

The decrease in FUS^{R521G} could be caused by a deficit in the synthesis, trafficking, and/or degradation of FUS proteins. To test whether FUS's response to DHPG stimulation is a local event at synapses, we isolated synaptoneurosomes using a discontinuous Percoll–sucrose gradient and treated them with DHPG in vitro. We found that FUS expression is induced significantly in the synaptoneurosomes of control mice (Fig. 5 *E* and *F*), suggesting that local synthesis of the protein does occur. We then performed these same in vitro experiments in synaptoneurosomes from CAG-FUS^{WT} and CAG-FUS^{R521G} mice. We found that both endogenous mouse FUS and exogenous human FUS^{WT} increase in the CAG-FUS^{WT} samples and decrease in the CAG-FUS^{R521G} samples (Fig. 5*G*), as is consistent with our observation in the acute cortical tissue slice model (Fig. 5 *C* and *D*). We then tested whether the decrease in FUS^{R521G} could be blocked using a proteasome inhibitor, MG132, and found that inhibiting the proteasome does not prevent a decrease in FUS expression (Fig. 5*H*). Together, these observations suggest that the alterations of FUS levels in response to mGluR activation are local synaptic events, likely related to protein synthesis.

Discussion

Cre-Inducible Transgenic Mice Expressing Low Levels of FUS as Novel Models of ALS and FTLD. The pathological and genetic association of FUS with ALS and FTLD suggests that dysregulation of FUS may lead to neurodegenerative diseases. However, the mechanism by which FUS aggregation or mutations cause ALS and FTLD is not known. To study the role of FUS in neurodegeneration, we generated Cre-inducible FUS transgenic mice that express low levels of wild-type (FUS^{WT}) or mutant (FUS^{R521G}) proteins. Under control of the CAG promoter, the human FUS transgene is expressed ubiquitously in the germ line of CAG-FUS^{WT} and CAG-FUS^{R521G} mice (Fig. 1). CAG-FUS^{WT} and CAG-FUS^{R521G} mice that develop severe deficits in motor function have denervation of the NMJs, muscle atrophy, neuroinflammation, and early lethality (Figs. 1 and 2). The phenotypes observed in our transgenic models phenocopy aspects of adult cases of ALS. However, the onset of phenotypes in the mouse models is earlier, more closely reflecting FUS-linked juvenile ALS (29–31).

A portion of CAG-FUS^{R521G} mice that escape early lethality have impairments in motor function and sociability (Figs. 1 *I–L* and 3), which are likely linked to the alterations in dendritic branches and spines in the upper and lower motor neurons (Figs. 4 and 5). Adult CAG-FUS^{R521G} mice do not perform as well on the rotorod and they are less active on a running wheel (Fig. 3 *A* and *B*). Specifically, the forelimbs of these mice are impaired (*SI Appendix*, Fig. S7 *E* and *F*). Upper or lower limb weakness is common in both ALS and FTLD with motor function deficits (32–35). Changes in social interactions also are

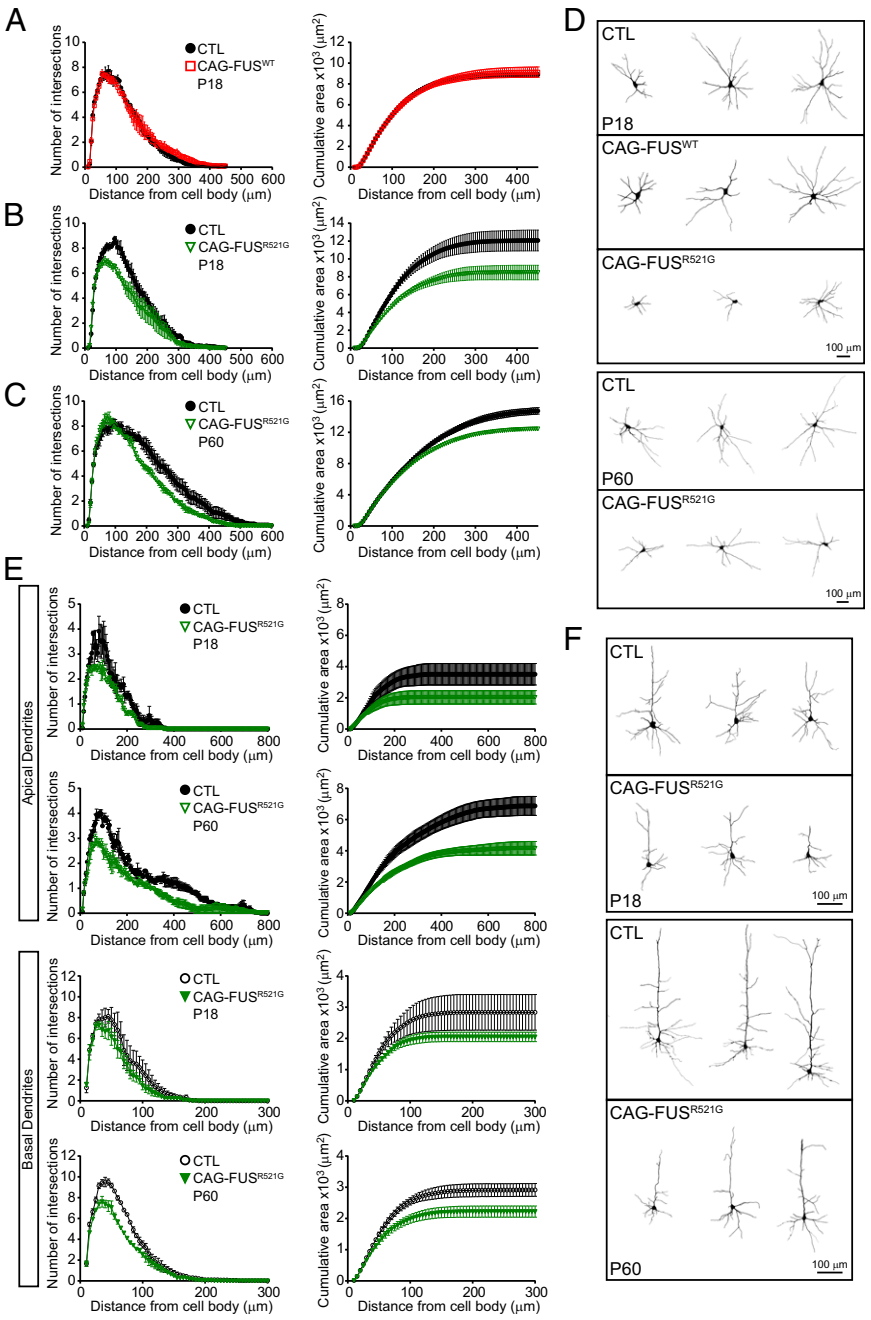

Fig. 4. Reduced dendritic branching in spinal motor neurons and sensorimotor neurons of CAG-FUS^{R521G} mice. (*A*) Sholl analyses show no reduction in the number of dendritic intersections or cumulative area of dendrites in spinal motor neurons in CAG-FUS^{WT} mice. (*B* and *C*) In contrast, the dendritic intersections and cumulative area of dendrites show significant reductions of spinal motor neurons in P18 (*B*) and in 2-mo-old (P60) (*C*) CAG-FUS^{R521G} mice. (*D*) Representative images of Neurolucida tracing of the dendrites of spinal motor neurons in control (CTL), CAG-FUS^{WT}, and CAG-FUS^{R521G} mice. A total of 36 spinal motor neurons were analyzed in CAG-FUS^{WT} and CAG-FUS^{R521G} mice and corresponding littermate controls. (*E, Upper*) Sholl analyses show reduced intersections and cumulative area in the apical dendrite within 50–250 μm from the cell body of cortical neurons of P18 and P60 CAG-FUS^{R521G} mice. (*Lower*) Similar reductions in the dendritic intersections and cumulative surface areas are also identified in the basal dendrites of CAG-FUS^{R521G} neurons. A total of 24 neurons from cortical layers IV–V were analyzed in CAG-FUS^{R521G} mice and corresponding littermate controls. (*F*) Representative images of Neurolucida tracing of the apical and basal dendrites in neurons from layers IV–V in the sensorimotor cortex in control and CAG-FUS^{R521G} mice. For each group three or four animals were analyzed. (*A–C* and *E*) $P < 0.0001$ (two-way repeated measures ANOVA). Error bars represent SEM.

a common clinical feature of patients with FTLD and in ALS patients with dementia (1). Similar to progranulin (*Grn*)-knockout mice, a model of familial FTLD that has deficits in social interaction (36), CAG-FUS^{R521G} mice have deficits in social interactions with intruder/novel juvenile and adult mice (Fig. 3 *E* and *F* and *SI Appendix*, Fig. S7*I*).

Differences and Commonalities in FUS Overexpression and Missense Mutations. The CAG-FUS^{WT} and CAG-FUS^{R521G} mouse models demonstrate that increased expression of FUS alone can cause cellular toxicity. This result is consistent with the recent finding that mutations in the 3′ UTR of *FUS* increase FUS expression levels and cause ALS (15). This result is also in agreement with

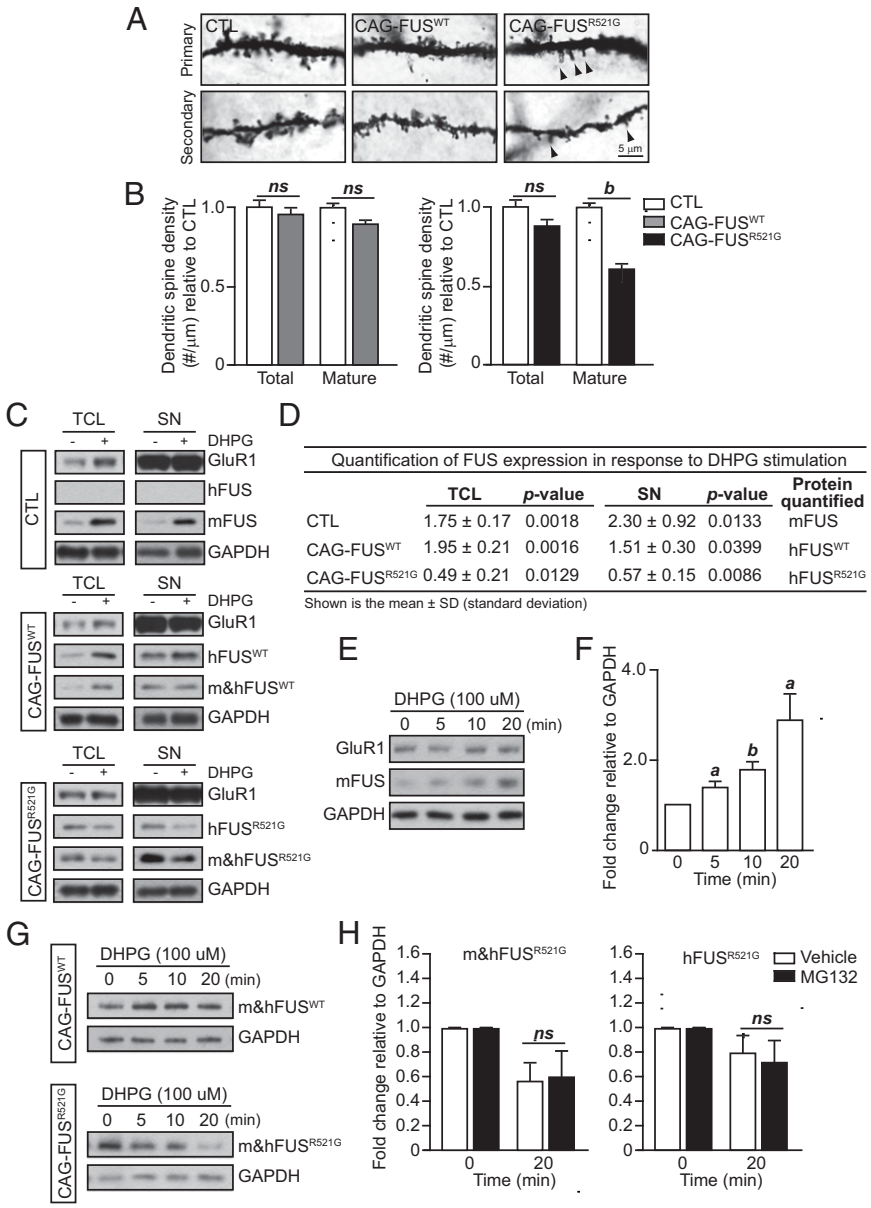

Quantification of FUS expression in response to DHPG stimulation

	TCL	*p*-value	SN	*p*-value	Protein quantified
CTL	1.75 ± 0.17	0.0018	2.30 ± 0.92	0.0133	mFUS
CAG-FUS^{WT}	1.95 ± 0.21	0.0016	1.51 ± 0.30	0.0399	hFUS^{WT}
CAG-FUS^{R521G}	0.49 ± 0.21	0.0129	0.57 ± 0.15	0.0086	hFUS^{R521G}

Shown is the mean ± SD (standard deviation)

Fig. 5. Activity-dependent reduction of FUS^{R521G} in response to mGluR stimulation. (*A* and *B*) Golgi images of dendritic spines in the apical and basal dendrites of control (CTL), CAG-FUS^{WT}, and CAG-FUS^{R521G} mice. Spine density was analyzed in a total of 30 neurons from cortical layers IV–V in P18 CAG-FUS^{WT} and CAG-FUS^{R521G} mice and their corresponding littermate controls ($n = 3$ mice per group). In CAG-FUS^{WT} mice the density of mature dendritic spines does not differ in apical and basal dendrites. However, in CAG-FUS^{R521G} mice the density of mature dendritic spines is reduced in the apical and secondary dendrites compared with littermate controls. (We have defined "mature" spines as being mushroom-shaped.) Arrowheads indicate immature spines. (*C*) Acute cortical tissue slices from littermate P18CTL, CAG-FUS^{WT}, or CAG-FUS^{R521G} mice ($n = 3$ mice per group) were pretreated with AMPA (20 μM 6,7-dinitroquinoxaline-2,3-dione, DNQX) and NMDA [5 μM 3-(2-carboxypiperazin-4-yl)propyl-1-phosphonic acid, CPP] inhibitors, followed by treatment with 100 μM DHPG for 10 min or no DHPG treatment. Total cell lysates (TCL) and synaptoneurosomes (SNs) were immunoblotted for human FUS (hFUS), mouse FUS (mFUS), total FUS (m&hFUS), GAPDH, and GluR1. GluR1 is enriched in the synaptoneurosome fraction. (*D*) Quantification of FUS expression from total cell lysates and synaptoneurosomes from acute cortical tissue slices treated with DHPG relative to untreated groups. Immunoblots are representative of three or four separate experiments. *P* values were obtained by Student *t* test. (*E*) Isolated synaptoneurosomes from CTL mice were treated with 100 μM DHPG for the indicated time and were immunoblotted for mFUS, GAPDH, and GluR1. (*F*) Quantification of FUS relative to GAPDH indicates a significant increase in expression in response to DHPG treatment. (*G*) Isolated synaptoneurosomes from CAG-FUS^{WT} and CAG-FUS^{R521G} mice were treated with 100 μM DHPG for the indicated time and were immunoblotted for total m&hFUS and GAPDH. Immunoblots are representative of two separate experiments. (*H*) Isolated synaptoneurosomes from CAG-FUS^{R521G} mice were pretreated with 25 μM MG132 or vehicle (DMSO) before stimulation with 100 μM DHPG for 20 min. Synaptoneurosome lysates were immunoblotted, and m&hFUS and hFUS levels were quantified relative to GAPDH. MG132 did not inhibit the decrease in FUS expression. (*B*, *D*, *F*, and *H*) ns, not significant. a, $P < 0.05$; b, $P < 0.01$ (Student *t* test). The FUS Santa Cruz antibody was used for all blots for m&hFUS. Three animals were used in each experimental group. (*B* and *H*) Error bars represent SEM; (*F*) Error bars represent SD.

the observations that increased gene dose or overexpression of APP, α-synuclein, and TDP-43 can cause Alzheimer's disease, Parkinson disease, and ALS/FTLD (16–18). On the other hand, we did not detect overt motor neuron loss or apparent ubiquitin-positive aggregation and mislocalization of FUS in neurons and glia of either of our transgenic mouse models (*SI Appendix*, Fig. S1 *E–H*), suggesting that permanent FUS mislocalization, aggregation, and motor neuron loss are not necessary for disease onset but might be

end-stage pathological markers or outcomes in human patients. Moreover, our studies suggest that peripheral and central synapses are more vulnerable than axons and cell bodies and that synaptic defects precede axonal and neuronal degeneration.

The cellular phenotypes observed in our animal models may represent cellular events occurring before FUS mislocalization, aggregation, and neuronal death that are the key neuropathological features of ALS/FTD. Although FUS^{R521G} is not overtly mislocalized in our animals, it is likely that the shuttling dynamics of FUS^{R521G} are altered, because FUS R521 residue is located at PY-NLS. On the other hand, PY-NLS has very high binding affinity (k_d = 9.5 nM) for karyopherinβ2 (Kapβ2, also known as "transportin"), which mediates FUS nuclear shuttling (37). Although ALS mutations in PY-NLS reduce Kapβ2-binding affinities by several fold (37), the mutant FUS proteins still have nanomolar affinity and thus are expected to be translocated efficiently to the nucleus unless the nuclear import machinery is overwhelmed (such as when wild-type or mutant FUS proteins are massively overexpressed). Therefore it is not surprising that there is no overt FUS mislocalization in our transgenic mice with low FUS expression.

Some of our CAG-FUS^{R521G} mutant mice escaped early lethality, but none of the CAG-FUS^{WT} mice survived to adulthood. The similar phenotypes we observe in both of the CAG-FUS^{WT} and CAG-FUS^{R521G} founding lines reduces the possibility that these observations are caused by insertional effects. Also, these transgenic lines have very low copy numbers of transgenes with single genomic insertion (*SI Appendix*, Fig. S1*C*). Interestingly, in ALS patients the age of disease onset and clinical phenotypes are variable, with incomplete penetrance for TDP-43 and FUS mutations. It is possible that other factors, such as genetics and environment, have an impact on whether an individual can escape the consequences of these autosomal dominant mutations. Incomplete penetrance has also has been observed in carriers of the APOE4 allele, 50% of whom develop Alzheimer's disease but the remainder do not. Another argument for incomplete penetrance of FUS mutations has to do with the possibility that mutations in the PY-NLS are also partial loss-of-function mutations, presumably in gene expression. This is supported by the finding that the ALS-associated FUS mutant proteins R521G and H517Q have reduced binding to intronic sequences of its nuclear RNA targets (24).

We note that the CAG-FUS^{WT} mice readily recapitulated human diseases caused by increased levels of wild-type FUS. Although CAG-FUS^{R521G} mice can model the toxic gain of functions of FUS (which is highly relevant to the studies of ALS/FTLD), modeling loss of function is more difficult in the mutant mice. Nevertheless, results from our parallel studies of the wild-type and mutant animals are consistent with a model wherein overexpression of FUS^{WT} alters the nuclear function of endogenous FUS at the level of gene expression, but FUS^{R521G} mutation has both a partial loss of function in RNA regulation and gene expression and a partial toxic gain of function in disrupting synapses. This model is supported by our transcriptome analysis of the spinal cords of the transgenic mice, which revealed that the gene-expression pattern is altered in CAG-FUS^{WT} mice but not in CAG-FUS^{R521G} mice (*SI Appendix*, Fig. S6). This result also potentially explains why an increase in wild-type FUS level is more deleterious than the overexpression of FUS^{R521G} (Fig. 1 and *SI Appendix*, Fig. S6 and Table S2). At the steady state, both FUS^{WT} and FUS^{R521G} stay mainly in the nucleus, but FUS^{R521G} has no apparent effect on gene expression. This result supports the view that overexpressed FUS^{R521G} has a diminished ability to alter the nuclear function of endogenous FUS in gene expression. As discussed in more detail in the next section, although FUS^{R521G} does not affect gene expression, it has a toxic gain of function disrupting synaptic homeostasis at dendritic spines. In contrast, FUS^{WT} does not affect synaptic homeostasis.

In other published animal models (38–40), overexpression of wild-type FUS has been reported as being less toxic than overexpression of mutant FUS. In addition, a recently developed FUS^{WT} transgenic mouse line showed no deficits until crossed to homozygosity, wherein these mice displayed progressive hindlimb paralysis and neuromuscular denervation (41). These studies contrast with our observation that overexpression of FUS^{WT} is more toxic than overexpression of FUS^{R521G} in terms of early lethality. The reason for the different degree of toxicity in different FUS transgenic models needs to be examined further and will yield important insight into disease progression. In this regard, we note that in our models FUS proteins are expressed globally at low levels and during early embryonic development. Because ALS is thought to be a non–cell-autonomous disease (42), it will be important to examine the contribution of different cell types, particularly astrocytes and microglia, to the phenotypes observed in our transgenic models. The Cre-inducible transgenic system developed herein will allow temporal and spatial expression of FUS proteins in glial cells to test the hypothesis that ALS and FTLD are non–cell-autonomous. Similarly, it will be informative to use Cre-lines specific for motor neurons and cortical neurons to examine separately FUS's contributions to ALS and FTLD.

Mutant-Specific Disruption of mGluR-Dependent Synaptic Homeostasis. Primary hippocampal cultures from FUS-knockout mice have altered dendritic branching and reduced mature spines (14). Based on this information and the behavioral phenotypes in the CAG-FUS^{R521G} mice, we examined dendritic branching in the motor neurons and sensorimotor cortex and found significant reductions in dendritic intersections and in the cumulative area of dendrites. Moreover, the density of mature dendritic spines is reduced in the apical and secondary dendrites in the mutant mice (Fig. 5). These data are consistent with transgenic mice harboring the R521C mutation under control of the Syrian hamster prion promoter (43). However, Qiu et al. (43) reported only transgenic mice for FUS mutant R521C, without comparable wild-type transgenic animals. Therefore it was unclear whether the phenotypes in their studies were caused by simple overexpression of FUS protein or were specific to the FUS mutation. In our studies we observed persistent dendritic defects in the spinal motor neurons and cortical neurons in FUS^{R521G} mice at P18 and P60, suggesting that the negative impacts of FUS^{R521G} on dendritic morphology can occur at young age. Importantly, we did not see the same alterations in the CAG-FUS^{WT} mice, indicating that although certain aspects of the CAG-FUS^{WT} and CAG-FUS^{R521G} models are similar, the alterations in synaptic homeostasis resulting in alterations in dendritic branches and spines are specific to the R521G mutation. It is likely that disruption of synaptic homeostasis at dendritic spines contributes to the alterations in motor function and social interaction of the mutant transgenic animals.

Interestingly, *Gm*-knockout mice display similar alterations in dendritic branching and spine maturation, which correspond with deficits in social interaction (36). FTLD and ALS share common clinical and pathological features including loss of cognition, motor impairment, and TDP-43– or FUS-positive inclusions. Although the FUS R521G mutation is associated with familial ALS, the rare FUS mutations P106L, G206S, and M254V are linked to familial FTLD (3). Indeed, our CAG-FUS^{R521G} mice phenocopy aspects of the loss of motor function observed in ALS. They also show changes in social interactions resembling those observed in FTLD. On the other hand, alterations in dendritic branching and spines have not been documented for ALS or FTLD, but the findings from our CAG-FUS^{R521G} mice suggest that these alterations might exist in human patients.

FUS also localizes to RNA granules at the synapse (27) and copurifies with the NMDA receptor (44). In response to mGluR5

stimulation, there is more immunodetectable FUS at dendritic spines (14). Fujii et al. (14) did not assess whether the increase in immunodetectable FUS at the synapse was caused by local translation of FUS mRNA or by localization to the synapse. Using an in vitro assay to assess local protein translation in isolated synaptoneurosomes, we demonstrate that the increase in FUS expression at the synapse in response to mGluR activation is a local event (Fig. 5 *E* and *F*). The acute increase in synaptic FUS expression in response to mGluR activation as demonstrated by Fujii et al. (14) and in our study strongly suggests that FUS participates in the regulation of mRNAs important to synaptic function and serves as an important synaptic RNA-binding protein. This finding is reproducible in our studies using acute cortical tissue slices, where FUS^{WT} protein is increased but FUS^{R521G} protein is reduced in response to mGluR activation (Fig. 5 *C* and *D*). We also found that inhibiting the proteasome does not prevent the activity-dependent decrease of FUS expression in synaptoneurosomes isolated from CAG-FUS^{R521G} mice. Together, these observations suggest that the alterations of FUS levels in response to mGluR activation are local synaptic events that are likely to be related to protein synthesis. Future studies will test whether dysregulation of synaptic FUS in response to mGluR activation contributes to the altered dendritic branching and maturation of spines in the CAG-FUS^{R521G} mice and perhaps also in human patients with ALS or FTLD.

Activity-dependent down-regulation of the FUS^{R521G} protein at the synapse and its potential role in disrupting the formation or maintenance of dendritic spines provides a tantalizing mechanism for FUS regulation at the synapse. In this context, we note that our finding that FUS dysfunction disrupts synaptic homeostasis at dendritic spines somewhat parallels observations for another RNA-binding protein, fragile X mental retardation protein (FMRP). FMRP has been shown to regulate spine shape in a protein synthesis-dependent manner. In response to mGluR signaling, FMRP regulates local translation of mRNAs at the synapse (45). Loss-of-function mutations in the *FMR1* gene cause fragile X mental retardation syndrome, in which a deficit in spine maturation is thought to underlie the autism-like symptoms in individuals with the syndrome (46). In the future, it would be important to test how deficits in the synthesis of mutant FUS proteins lead to the disruption of synaptic homeostasis. Moreover, it would be of interest to examine whether disruption of synaptic homeostasis caused by dysfunction of RNA metabolism represents a common theme of brain disorders.

Materials and Methods

For more details, see *SI Appendix, Supplemental Experimental Procedures*.

Generation of FUS Transgenic Mice. Wild-type or mutant R521G human FUS cDNAs were inserted into the CAG-Z-IRES-EGFP vector (provided by Yuji Mishina, University of Michigan, Ann Arbor, MI). The CAG-Z-FUS-IRES-EGFP construct was digested with *AflII* and *SpeI* to remove the vector sequence and then was injected into fertilized oocytes from C57BL/6 female mice and implanted into pseudopregnant ICR mice. Mice carrying the transgene were identified by PCR analysis and β-galactosidase activity as previously reported (47). To induce global overexpression of human FUS, the *CAG-Z-FUS-IRES-EGFP* mice were bred to Meox2-Cre mice to yield CAG-FUS^{WT} or CAG-FUS^{R521G} mice. CAG-FUS^{WT} and CAG-FUS^{R521G} pups were monitored daily and scored as follows: 0 = healthy; 1 = limp tail or hindlimb weakness; 2 = limp tail and hindlimb weakness; 3 = moderate hindlimb weakness and/or unilateral hindlimb paralysis; 4 = bilateral, complete hindlimb paralysis; and 5 = moribund state accompanied by complete hindlimb paralysis with forelimb weakness. Mice with a score of 3 or higher or that had a loss of total body weight >20, were considered to have reached end stage and were euthanized. All experimental procedures involving animals in this study were reviewed and approved by the University of Texas Southwestern Institutional Animal Care and Use Committee.

Behavior Testing. ***Grip test.*** Mice were placed on a 15.5 × 15.5-cm wire grid. The grid then was inverted and secured 42 cm above a padded surface. Latency to fall was measured, with a maximum trial time of 1 min. The latency to fall is reported for P12–P30 CAG-FUS^{WT} (n = 21 litters) and CAG-FUS^{R521G} (n = 17 litters) transgenic mice and their littermate controls.

Rotorod. Mice were placed on a stationary rotorod (IITC Life Science Inc.). The rod then was accelerated from 5–45 rpm over 5 min. The time that each mouse fell from the rod was recorded. Mice that held onto the rod for two complete rotations were scored as if they had fallen from the rod. Each mouse was tested four times a day for two consecutive days with an intertrial interval of at least 15 min. CAG-FUS^{R521G} (Tg/+;Cre/+, n = 18) and littermate controls (Tg/+;$^{+/+}$, n = 19 and $^{+/+}$;Cre/+, n = 19) were tested.

Running wheel. Mice were housed individually in running-wheel cages with access to food ad libitum. Wheel-running activity was recorded continuously for 14 d using the ClockLab data collection system (Actimetrics). Locomotor activity was assessed in the final 9 d of recording, allowing acclimation to the running wheel. CAG-FUS^{R521G} (n = 6) and littermate controls (n = 4) were tested at 5 mo of age.

Digigait. Mice were placed onto the Digigait (Mouse Specifics) and allowed to explore and habituate for 2–3 min. Then the treadmill was started at 10 cm/s, and the speed was increased rapidly to 20 cm/s. A camera located below the transparent treadmill collected the images, and the data were analyzed automatically by the software. Approximately 10 steps at a constant pace were recorded. CAG-FUS^{R521G} (Tg/+;Cre/+, n = 18) and littermate controls (Tg/+;$^{+/+}$, n = 19 and $^{+/+}$;Cre/+, n = 19) were tested at 2 mo of age.

Resident/intruder test. Adult test mice were housed singly in clean cages for 24 h before testing. An adult intruder/novel mouse (age 3–8 mo, same sex as the test mouse and not heavier) was introduced into the cage containing the resident/test mouse. Each trial duration was 10 min, and active behaviors were recorded using the Noldus Observer program. Active behaviors were defined as attack (resident biting, pinning, and kicking of the hind limbs), chase (resident closely following the intruder), grooming (resident climbing on intruder, tugging its hair or tail, or rubbing its snout on the intruder's body), and sniffing (resident sniffing the intruder's anogenital region or other body part). Intruder mice were used only twice. Acclimation and testing were conducted under red light to minimize any stress and anxiety. CAG-FUS^{R521G} (Tg/+;Cre/+, n = 17) and littermate controls (Tg/+;$^{+/+}$, n = 15 and $^{+/+}$;Cre/+, n = 16) were tested at 8 mo of age.

Histology Staining. Tissues stained with H&E were fixed in 10% (wt/vol) formalin fixative for 48 h, paraffin embedded, and sectioned to 8-μm thickness.

Immunostaining. Brains, spinal cords, and NMJs from whole mounts of triangularis sterni muscles from mice (age P18–P25) were prepared and immunostained as previously described (47–49). Tissue sections were immunostained with primary antibodies: GFAP (AB5541; Millipore), IBA1 (019-19741; Wako), GFP (Aves 1020), human FUS (B327D), and To-Pro3 (T3605; LifeTechnologies). Triangularis sterni muscles were immunostained with Alexa Fluor 647 α-bungarotoxin (AchR; Invitrogen) or Syntaxin 1 (a gift from Thomas Südhof, Stanford University, Stanford, CA). Primary antibodies were incubated overnight at 4 °C, and Alexa Fluor-conjugated secondary antibodies (Invitrogen) were incubated for 2 h at room temperature. Three animals from each genotype (n = 3) were analyzed, and a minimum of 400 NMJs per genotype were assessed.

Western Blot Analysis. Lysates from tissues were processed, and equal proteins were resolved by SDS/PAGE as previously reported (47). Primary antibodies used were glutamate receptor 1 (GluR1; MAB2263; Millipore), GAPDH (G9545; Sigma), FUS (HPA008784; Sigma), FUS (sc-47711; Santa Cruz), GFP (1020; Aves); human FUS antibody was a gift from Hongxia Zhou and Xu-Gang Xia, Thomas Jefferson University, Philadelphia (40) and human FUS peptide antibody B327D (SYGQPQSGSYSQQPS) was generated in rabbits as previously described (47). Immunodetected proteins were quantified by densitometry using the NIH ImageJ software. We were able to estimate the amounts of human and mouse FUS in the transgenic animals visually by using larger SDS/PAGE gels (Fig. 1*D*) but were unable to quantify the human FUS level accurately because of the similar molecular weights of human FUS (526 amino acids) and mouse FUS (518 amino acids) (*SI Appendix*, Fig. S1*D*).

Golgi Staining for the Analysis of Dendrites in Cortical Neurons and Cervical Spinal Motor Neurons. Both male and female CAG-FUS^{WT} and CAG-FUS^{R521G} mice and their littermate controls were used for Golgi staining, and samples were analyzed used the Neurolucida software (MicroBrightField) as previously reported (43). Three animals from each genotype (n = 3), with 12 cervical spinal motor neurons (from the ventral horn region) and 10 cortical neurons (from layers IV–V in the sensorimotor cortex) were traced and analyzed.

Choline Acetyltransferase Staining of Spinal Cord and Quantification of Spinal Motor Neurons. Tissues from the cervical spinal cord were processed, immunostained, and analyzed as previously reported (43). Anti-choline

acetyltransferase (ChAT) (1:300; Millipore), biotinylated rabbit anti-goat IgG antibody (1:100; Vector Labs); and the VECTASTAIN Elite ABC Kit (Vector Labs) were used for staining motor neurons. ChAT-positive cells in the ventral horn region were quantified using at least 12 images per animal. CAG-FUS^{R521G} ($n = 3$) and CAG-FUS^{WT} ($n = 4$) transgenic mice and their littermate controls ($n = 3$ or 4) were analyzed.

Acute Treatment of Cortical Tissue Slices with DHPG. After DHPG treatment of acute cortical tissue slices, total cell lysates were collected, and the remaining homogenate was passed through two 100-μm filters and then through one 10-μm filter. Synaptoneurosomes were pelleted after 10-min centrifugation at 1,000 × *g*. Total cell lysates, supernatants, and synaptoneurosomes were lysed as previously reported (50). Experimental replicates ($n = 3$) were analyzed for each genotype.

Synaptoneurosome Isolation, in vitro Treatment with DHPG. Synaptoneurosomes used for in vitro DHPG stimulation experiments were isolated as previously reported (51). Synaptoneurosomes were equilibrated to room temperature for 10 min before stimulation with DHPG (100 μM). Pretreatment with DMSO (vehicle) or 25 μM MG132 (Tocris Biosciences) was performed at room temperature for 10 min before DHPG stimulation.

ACKNOWLEDGMENTS. We thank Jim Richardson and John Shelton of the University of Texas Southwestern (UTSW) Histology Core Facilities for assistance with histology staining and analysis; Shari Birnbaum and Laura Peca of the UTSW Behavior Core Facility for assistance with rotorod, Digigait, social interaction, olfactory, and Y-test testing; Erik Plautz and Sherry Rovinsky of the UTSW Neuro-Models Facility, with support from the Haggerty Center for Brain Injury and Repair, for assistance with ladder-rung testing and analysis; Leighton Stein of the Roswell Park Cancer Institute for assistance with FISH analysis of copy number in mouse embryonic fibroblasts; Weichun Lin for advice on NMJ studies; Vincent Zimmern (Ecole Polytechnique Federale de Lausanne) and Pradipta Ray (University of Texas at Dallas) for contributions to the initial RNA-Seq analysis; and Paul A. Dutchak for experimental discussion and critical feedback on the manuscript. This work was supported by Alzheimer's Association, Consortium for Frontotemporal Dementia Research, Friends of the Alzheimer's Disease Center of UT Southwestern Medical Center, National Institutes of Health, National Natural Science Foundation of China, Ministry of Science and Technology of China, US Department of Veterans Affairs Biomedical Laboratory Research and Development Merit and Pilot Awards, and Muscular Dystrophy Association.

1. Lomen-Hoerth C, Anderson T, Miller B (2002) The overlap of amyotrophic lateral sclerosis and frontotemporal dementia. *Neurology* 59(7):1077–1079.
2. Mackenzie IR, et al. (2010) Nomenclature and nosology for neuropathologic subtypes of frontotemporal lobar degeneration: An update. *Acta Neuropathol* 119(1):1–4.
3. Dormann D, Haass C (2013) Fused in sarcoma (FUS): An oncogene goes awry in neurodegeneration. *Mol Cell Neurosci* 56:475–486.
4. Lee EB, Lee VM, Trojanowski JQ (2012) Gains or losses: Molecular mechanisms of TDP43-mediated neurodegeneration. *Nat Rev Neurosci* 13(1):38–50.
5. Tan AY, Manley JL (2009) The TET family of proteins: Functions and roles in disease. *J Mol Cell Biol* 1(2):82–92.
6. Burd CG, Dreyfuss G (1994) Conserved structures and diversity of functions of RNA-binding proteins. *Science* 265(5172):615–621.
7. Lerga A, et al. (2001) Identification of an RNA binding specificity for the potential splicing factor TLS. *J Biol Chem* 276(9):6807–6816.
8. Iko Y, et al. (2004) Domain architectures and characterization of an RNA-binding protein, TLS. *J Biol Chem* 279(43):44834–44840.
9. Kato M, et al. (2012) Cell-free formation of RNA granules: Low complexity sequence domains form dynamic fibers within hydrogels. *Cell* 149(4):753–767.
10. Lee BJ, et al. (2006) Rules for nuclear localization sequence recognition by karyopherin beta 2. *Cell* 126(3):543–558.
11. Dormann D, et al. (2012) Arginine methylation next to the PY-NLS modulates Transportin binding and nuclear import of FUS. *EMBO J* 31(22):4258–4275.
12. Dormann D, Haass C (2011) TDP-43 and FUS: A nuclear affair. *Trends Neurosci* 34(7):339–348.
13. Bentmann E, et al. (2012) Requirements for stress granule recruitment of fused in sarcoma (FUS) and TAR DNA-binding protein of 43 kDa (TDP-43). *J Biol Chem* 287(27):23079–23094.
14. Fujii R, et al. (2005) The RNA binding protein TLS is translocated to dendritic spines by mGluR5 activation and regulates spine morphology. *Curr Biol* 15(6):587–593.
15. Sabatelli M, et al. (2013) Mutations in the 3′ untranslated region of FUS causing FUS overexpression are associated with amyotrophic lateral sclerosis. *Hum Mol Genet* 22(23):4748–4755.
16. Gitcho MA, et al. (2009) TARDBP 3′-UTR variant in autopsy-confirmed frontotemporal lobar degeneration with TDP-43 proteinopathy. *Acta Neuropathol* 118(5):633–645.
17. Rovelet-Lecrux A, et al. (2006) APP locus duplication causes autosomal dominant early-onset Alzheimer disease with cerebral amyloid angiopathy. *Nat Genet* 38(1):24–26.
18. Chartier-Harlin MC, et al. (2004) Alpha-synuclein locus duplication as a cause of familial Parkinson's disease. *Lancet* 364(9440):1167–1169.
19. Kwiatkowski TJ, Jr, et al. (2009) Mutations in the FUS/TLS gene on chromosome 16 cause familial amyotrophic lateral sclerosis. *Science* 323(5918):1205–1208.
20. Vance C, et al. (2009) Mutations in FUS, an RNA processing protein, cause familial amyotrophic lateral sclerosis type 6. *Science* 323(5918):1208–1211.
21. Schwartz JC, et al. (2012) FUS binds the CTD of RNA polymerase II and regulates its phosphorylation at Ser2. *Genes Dev* 26(24):2690–2695.
22. Ishigaki S, et al. (2012) Position-dependent FUS-RNA interactions regulate alternative splicing events and transcriptions. *Sci Rep* 2:529.
23. Rogelj B, et al. (2012) Widespread binding of FUS along nascent RNA regulates alternative splicing in the brain. *Sci Rep* 2:603.
24. Hoell JI, et al. (2011) RNA targets of wild-type and mutant FET family proteins. *Nat Struct Mol Biol* 18(12):1428–1431.
25. Lagier-Tourenne C, et al. (2012) Divergent roles of ALS-linked proteins FUS/TLS and TDP-43 intersect in processing long pre-mRNAs. *Nat Neurosci* 15(11):1488–1497.
26. Kwon I, et al. (2013) Phosphorylation-regulated binding of RNA polymerase II to fibrous polymers of low-complexity domains. *Cell* 155(5):1049–1060.
27. Belly A, Moreau-Gachelin F, Sadoul R, Goldberg Y (2005) Delocalization of the multifunctional RNA splicing factor TLS/FUS in hippocampal neurones: Exclusion from the nucleus and accumulation in dendritic granules and spine heads. *Neurosci Lett* 379(3):152–157.
28. Vanderklish PW, Edelman GM (2002) Dendritic spines elongate after stimulation of group 1 metabotropic glutamate receptors in cultured hippocampal neurons. *Proc Natl Acad Sci USA* 99(3):1639–1644.
29. Conte A, et al. (2012) P525L FUS mutation is consistently associated with a severe form of juvenile amyotrophic lateral sclerosis. *Neuromuscul Disord* 22(1):73–75.
30. Belzil VV, et al. (2012) Novel FUS deletion in a patient with juvenile amyotrophic lateral sclerosis. *Arch Neurol* 69(5):653–656.
31. Zou ZY, et al. (2013) De novo FUS gene mutations are associated with juvenile-onset sporadic amyotrophic lateral sclerosis in China. *Neurobiol Aging* 34(4):1312.e1–1312.e8.
32. Lee EB, et al. (2013) Topography of FUS pathology distinguishes late-onset BIBD from aFTLD-U. *Acta Neuropathologica Comm* 1(9):1–11.
33. Taieb G, et al. (2013) R521C mutation in the FUS/TLS gene presenting as juvenile onset flail leg syndrome. *Muscle Nerve* 48(6):993–994.
34. Rademakers R, et al. (2010) Fus gene mutations in familial and sporadic amyotrophic lateral sclerosis. *Muscle Nerve* 42(2):170–176.
35. Corrado L, et al. (2010) Mutations of FUS gene in sporadic amyotrophic lateral sclerosis. *J Med Genet* 47(3):190–194.
36. Petkau TL, et al. (2012) Synaptic dysfunction in progranulin-deficient mice. *Neurobiol Dis* 45(2):711–722.
37. Zhang ZC, Chook YM (2012) Structural and energetic basis of ALS-causing mutations in the atypical proline-tyrosine nuclear localization signal of the Fused in Sarcoma protein (FUS). *Proc Natl Acad Sci USA* 109(30):12017–12021.
38. Lanson NA, Jr, et al. (2011) A Drosophila model of FUS-related neurodegeneration reveals genetic interaction between FUS and TDP-43. *Hum Mol Genet* 20(13):2510–2523.
39. Murakami T, et al. (2012) ALS mutations in FUS cause neuronal dysfunction and death in Caenorhabditis elegans by a dominant gain-of-function mechanism. *Hum Mol Genet* 21(1):1–9.
40. Huang C, et al. (2011) FUS transgenic rats develop the phenotypes of amyotrophic lateral sclerosis and frontotemporal lobar degeneration. *PLoS Genet* 7(3):e1002011.
41. Mitchell JC, et al. (2013) Overexpression of human wild-type FUS causes progressive motor neuron degeneration in an age- and dose-dependent fashion. *Acta Neuropathol* 125(2):273–288.
42. Ilieva H, Polymenidou M, Cleveland DW (2009) Non-cell autonomous toxicity in neurodegenerative disorders: ALS and beyond. *J Cell Biol* 187(6):761–772.
43. Qiu H, et al. (2014) ALS-associated mutation FUS-R521C causes DNA damage and RNA splicing defects. *J Clin Invest* 124(3):981–999.
44. Husi H, Ward MA, Choudhary JS, Blackstock WP, Grant SG (2000) Proteomic analysis of NMDA receptor-adhesion protein signaling complexes. *Nat Neurosci* 3(7):661–669.
45. Darnell JC, Klann E (2013) The translation of translational control by FMRP: Therapeutic targets for FXS. *Nat Neurosci* 16(11):1530–1536.
46. Irwin SA, Galvez R, Greenough WT (2000) Dendritic spine structural anomalies in fragile-X mental retardation syndrome. *Cereb Cortex* 10(10):1038–1044.
47. Sephton CF, et al. (2010) TDP-43 is a developmentally regulated protein essential for early embryonic development. *J Biol Chem* 285(9):6826–6834.
48. Liu Y, Sugiura Y, Lin W (2011) The role of synaptobrevin1/VAMP1 in Ca2+-triggered neurotransmitter release at the mouse neuromuscular junction. *J Physiol* 589(Pt 7):1603–1618.
49. Dewey CM, et al. (2011) TDP-43 is directed to stress granules by sorbitol, a novel physiological osmotic and oxidative stressor. *Mol Cell Biol* 31(5):1098–1108.
50. Sephton CF, et al. (2011) Identification of neuronal RNA targets of TDP-43-containing ribonucleoprotein complexes. *J Biol Chem* 286(2):1204–1215.
51. Westmark PR, Westmark CJ, Jeevananthan A, Malter JS (2011) Preparation of synaptoneurosomes from mouse cortex using a discontinuous percoll-sucrose density gradient. *J Vis Exp*, 10.3791/3196.

SUPPLEMENTAL INFORMATION

Dysregulation of FUS Disrupts Synaptic Homeostasis

Chantelle F. Sephton, Amy A. Tang, Ashwinikumar Kulkarni, James West, Mieu Brooks, Jeremy J. Stubblefield, Yun Liu, Michael Q. Zhang, Carla B. Green, Kimberly M. Huber, Eric J. Huang, Joachim Herz, Gang Yu

SUPPLEMENTAL EXPERIMENTAL PROCEDURES

Immunostaining. Mice (ages P18-P25) were anesthetized and were transcardially perfused with 4% paraformaldehyde (PFA, wt/vol) dissolved in 1X phosphate-buffered saline (PBS) and post-fixed in 4% PFA (wt/vol) overnight at 4°C. Tissues were washed extensively in 1X PBS, dehydrated in 30% sucrose (wt/vol) and frozen in OCT. Tissue sections of 15 μM were immunostained with primary antibodies GFAP (Millipore, AB5541), IBA1 (Wako, 019-19741), GFP (Aves 1020), human FUS (B327D) FUS (Santa Cruz, sc-47711), FUS (Sigma, HPA008784), Ubiquitin (Abcam, Ab7780) or To-Pro3 (LifeTechnologies T3605) followed by Alexa Fluor®-conjugated secondary antibodies (Invitrogen). Primary antibodies were incubated overnight at 4°C and Alexa Fluor®-conjugated secondary antibodies (Invitrogen) were incubated for 2 hours at room temperature.

Whole mounts of triangularis sterni muscles of mice (P18-P25) were fixed in 2% PFA (wt/vol) in 0.1 M phosphate buffer (pH 7.3) for 1 hr at room temperature. The samples were blocked in dilution buffer (500 mM NaCl, 0.01 M phosphate buffer, 3% bovine serum albumin (wt/vol) and 0.01% thimerosal, then incubated for 30 min with Alexa Fluor® 647 α-bungarotoxin (Invitrogen) followed by overnight incubation at 4°C with antibodies: GFP (Aves 1020), Syntaxin 1, or S100 (Dako, Z0311). After extensive washes, muscle whole mounts were incubated with Alexa Fluor®-conjugated secondary antibody (Invitrogen). Samples were then washed with 1X PBS and mounted in VECTASHIELD mounting medium (Vector Laboratories). Images were acquired using a Zeiss LSM 510 confocal microscope. Three animals from each genotype (n=3) were analyzed and a minimum of 400 NMJs per genotype were assessed.

Western blot analysis. Tissues were homogenized in lysis buffer (10mM HEPES, pH 7.4, 4M Urea, 1% LDS (wt/vol), 1X protease cocktail inhibitor (Roche) in lysing matrix D tubes, using the FastPrep homogenizer (Millipore). Lysates were clarified by centrifugation at 20,000 x g for 30 min at 4°C. Protein concentration was determined by BCA assay (Themo Scientific), and equivalent amounts were resolved by SDS-PAGE and immunoblotted by a standard protocol. GAPDH (Sigma, G9545), FUS (Sigma, HPA008784), FUS (Santa Cruz (SC), sc-47711) and GFP (Aves, 1020) were used as primary antibodies. Quantification of western blots by densitometry was done using the NIH ImageJ software. Each sample was normalized to GAPDH. Affinity purified Human FUS antibodies were a gift from Hongxia Zhou at Thomas Jefferson University (1). Human FUS peptide antibodies B327D (SYGQPQSGSYSQQPS) were generated in rabbits as previously described (2). Note that although we were able to visually estimate the amounts of human and mouse FUS in the transgenic animals by using larger SDS-PAGE gels (Figure 1D), we were unable to accurately quantify human FUS level

due to the similar molecular weights between human FUS (526 amino acids) and mouse FUS (518 amino acids) (Figure S1D).

Li-Cor Odyssey. Equal protein lysates were resolved by SDS-PAGE and transferred to Immobilon® FL PVDF membrane (Millipore IPFL00010). Blots were then rinsed with MiliQ water and blocked using Odyssey blocking buffer (Li-Cor P/N: 927-40000). Blots were probed with following primary antibodies in Odyssey blocking buffer: Arc (Synaptic Systems, 156003), CamKII (Santa Cruz, sc-5391), GluR1 (Millipore, MAB2263), and Psd-95 (Thermo, MA1-0145). Following primary antibody incubation, blots were probed with IR Dye 800CW goat anti-rabbit (Li-Cor P/N: 827-08365), IR Dye 800CW donkey anti-goat (Li-Cor P/N: 926-32214), IR Dye 800CW goat anti-mouse (Li-Cor P/N: 827-08364) and IR Dye 680RD goat anti-mouse (Li-Cor P/N: 926-68170) respectively. Blots were imaged using Li-Cor Odyssey imaging system and quantified using Li-Cor Image Studio software.

Golgi staining for the analysis of dendrites in cortical neurons and cervical spinal motor neurons. Both male and female CAG-FUS^{WT} and CAG-FUS^{R521G} transgenic mice and their littermate controls were used for this analysis. Golgi staining on brains and cervical spinal cords from postnatal day 18 (P18) wild-type and CAG-FUS^{WT} or CAG-FUS^{R521G} littermate mice was performed using the Rapid GolgiStain Kit (FD Neurotechnologies) following the manufacturer's instructions. Briefly, brains and spinal cords from P18 mice were removed and immersed in solutions A and B in the dark for 2 weeks at room temperature. Brains were then transferred into solution C for at least 48 h at 4°C, sectioned at 100 μm thickness using a cryostat, mounted onto 3% gelatin-coated slides (wt/vol) and developed following the manufacturer's protocol (3).

Dendritic tracing was performed using Neurolucida software (MicroBrightField, Williston, VA) with Olympus BX51 and a 60X objective. Neurons were traced with the center of the soma as a focal point. Three animals from each genotype (n=3) were analyzed, with 12 cervical spinal motor neurons (from ventral horn region) and 10 cortical neurons (from layers IV-V in the sensorimotor cortex) randomly selected and analyzed from regions of interest. Neurolucida Explorer 10 software (MicroBrightField, Williston, VA) was used to perform Sholl analysis to determine the number of intersections, cumulative surface area and to generate representative Golgi-tracing neurons (3).

Counting of the dendritic spines in the apical dendrites of the cortical motor neurons was performed using Neurolucida and analyzed with NeuroExplorer software (3). Briefly, beginning with a radius of 30 μm away from the center of the soma, a total distance of 100 μm from the primary apical dendrite was traced and analyzed. The entire length of the immediate secondary apical dendrite attached to the primary dendrite was also traced and analyzed for the study. Three animals from each genotype (n=3) were analyzed, with 10 primary and secondary branches from each animal traced and analyzed.

ChAT staining of spinal cord and quantification of spinal motor neurons. Tissues were fixed with 4% PFA (wt/vol) and sectioned at 40 μm thickness and free-floated in 1X PBS. Free-floating sections were treated with antigen retrieval solution (10 mM sodium citrate buffer) at 95°C for 10 min, washed three times in 1X TBS, and

then incubated in blocking solution (5% goat serum (wt/vol), 0.1% Triton X-100 in 1X TBS) for 1 hour at room temperature. DAB staining of the floating sections was then performed. The following antibodies and reagents were used: anti-choline acetyltransferase (ChAT)(Millipore), biotinylated rabbit anti-goat IgG antibody (Vector Labs); VECTASTAIN Elite ABC Kit (Vector Labs). DAB stained sections were mounted onto slides with Permount. Bright-field images of the ventral horns were captured using a 10X objective on an Olympus BX53 and on an Olympus DP72 digital camera. ChAT positive cells were quantified in each image field of the ventral horn region, and a minimum of 12 images for each animal were examined. CAG-FUS^{R521G} (n=3) and CAG-FUS^{WT} (n=4) transgenic mice and their littermate controls (n=3-4) were analyzed.

Acute cortical tissue slices, treatment with DHPG and synaptoneurosome isolation. Treatment of acute cortical tissue slices and isolation of synaptoneurosomes (SNs) from P18 mice were performed similar to previously reported (4). P18 mice were anesthetized with pentobarbital, whole brains were dissected out and immersed into ice cold oxygenated dissection buffer (110 mM choline Cl, 2.5 mM KCl, 1.25 mM NaH_2PO_4, 25 mM $NaHCO_3$, 25 mM D-glucose, 3.1 Na pyruvate, 11.6 Na ascorbate, 14 mM $MgCl_2$, 0.5 mM $CaCl_2$). Acute slices of neocortex were taken at 400 μm thickness and recovered in normal artificial cerebrospinal fluid (ACSF; 125 mM NaCl, 2.5 mM KCl, 1.25 mM NaH_2PO_4, 25 mM $NaHCO_3$, 10 mM dextrose, 2 mM $MgSO_4$-anhydrous, 2 mM $CaCl_2$-2H2O) for 35 minutes in a 35°C, oxygenated water bath. Slices were then transferred to SN recovery buffer containing AMPA (20 μM DNQX) and NMDA (5 μM CPP) inhibitors and pretreated for 30 minutes before stimulation with DHPG (100 μM, 10 minutes) (Tocris, Biosciences, US). Cortical slices were then transferred to 1 ml ice-cold homogenization buffer (10 mM HEPES, 1 mM EDTA, 2 mM EGTA, 0.5 mM DTT, 1X Roche Protease inhibitors) and homogenized using a Dounce homogenizer (10 strokes with A and 10 strokes with B). Total cell lysates (TLC) were collected and the remainder was passed through two 100 μm filters followed by one 10 μm filter. SNs were pelleted after a 10 min centrifugation at 1000 x g. TCL, Supernatants, and SNs were lysed in lysis buffer as previously described (5). Experimental replicates (n=4) were analyzed for each genotype CAG-FUS^{WT}, CAG-FUS^{R521G}.

Synaptoneurosome isolation, *in vitro* treatment with DHPG. Brain cortices from P16 mice were removed, washed in ice-cold gradient medium (GM buffer: 0.25 M sucrose, 5 mM Tris-HCl, pH 7.5, and 0.1 mM EDTA), transferred to a glass Dounce homogenizer containing ice cold GM buffer, and gently homogenized with ten strokes of the loose pestle followed by ten strokes of the tight pestle. Cellular debris and nuclei were pelleted from the homogenate by centrifugation at 1000 x g for 10 min at 4°C. The supernatant was applied to percoll gradients (layers 2 ml each of 23%, 15%, 10%, and 3% isosmotic percoll, vol/vol) and spun at speed (32,500 x g) for 5 min at 4°C. The third band from the top of the gradient (the 23%/15% interface) containing intact SNs was removed and pooled for the experiments. The salt concentration of the SNs was adjusted by adding one-tenth volume of 10X stimulation buffer (100 mM Tris-HCl, pH 7.5, 5 mM Na2HPO4, 4mM KH2PO4, 40 mM NaHCO3, 800 mM NaCl). To suppress nonspecific excitation, tetrodotoxin (Tocris, Biosciences, US) to 1 μM was added. SNs were equilibrated to room temperature by rotation on a nutator mixer for 10 minutes, samples

were then placed at 37°C and stimulated with DHPG (100 μM) for the times indicated. All samples were incubated at 37°C for the same total time. Pretreatment of DMSO (vehicle) or 25 μM MG132 (Tocris, Biosciences, US) occurred at room temperature for 10 minutes prior to DHPG stimulation.

Toluidine blue staining. Mice were anesthetized and transcardially perfused with 4% PFA (wt/vol) and 1% glutaraldehyde (wt/vol) dissolved in 0.1M cacodylate, pH7.4. Tissues were post-fixed in 2.5% glutaraldehyde dissolved (wt/vol) in 0.1M cacodylate, pH7.4. Tissues were then post-fixed in buffered 1% osmium tetroxide (wt/vol) for 2 changes of 90 minutes each. Tissues were rinsed with dH_2O, en bloc stained in 4% uranyl acetate (vol/vol) in 50% ethanol, dehydrated with a graded series of ethanol, and embedded in EMbed-812 resin. 1 μm semi-thin sections of the L4 spinal cord and dorsal and ventral roots were taken and stained with 1% toluidine blue (wt/vol).

Counting Alpha Motor Neurons. Alpha motor neurons were counted in spinal cord sections prepared from mice after perfusion with 4% PFA (wt/vol). Samples were paraffin-embedded, sectioned serially (10 μm) onto 10 slides, and stained with cresyl violet. Motor neurons were counted in every 10th section through each population examined. Alpha motor neurons were chosen based on the criteria: 1) located in the ventral horns (right and left) of the spinal cord; 2) 80-100 μm in size; 3) containing large soma; 4) containing a clear nucleus with intact nuclear membrane; and 5) having at least one clump of nucleolar material.

Juvenile Social Interaction. Adult mice were placed into a clean, empty mouse cage for approximately 15 min to habituate to the cage. A novel juvenile mouse (3-4 weeks, same sex as the test mouse) was then introduced into the cage and the total time that the adult mouse interacted with the juvenile was recorded. Trial duration was 2 min. All tests were conducted under red light in order to minimize any stress and anxiety. CAG-FUS^{R521G} (Tg/+;Cre/+, n=18) and littermate controls (Tg/+;+/+, n=19 and +/+;Cre/+, n=19) were tested at 2, 4, 6 and 8 months of age.

Ladder Walking Test. This task was used to evaluate fine motor skills involved in performing accurate stepping behavior (6, 7). The task apparatus and scoring system were adapted from Farr et al. (2006) and Tennant & Jones (2009). The horizontal ladder (Plexiglas walls, 81 cm long, 15 cm tall, elevated 25 cm from ground) was composed of 0.15 cm diameter metal rungs spaced evenly 1.5 cm apart. Animals performed 3 trials (crossings) on a single test day (inter-trial interval at least 10 min). Video was analyzed frame-by-frame for step quality according to a 0-6 point scale. Scores of 0-2 indicated varying severity of slips, with scores of 3-5 indicating lesser types of missteps, and a score of 6 indicating an ideal paw placement. Two values were derived from this analysis: a step score (average of all scored steps) and an error rate (count of steps scored 0-2 divided by total step count). Forelimb and hindlimb scores were tallied separately; scores from right/left limbs were pooled. CAG-FUS^{R521G} (Tg/+;Cre/+, n=10) and littermate controls (Tg/+;+/+, n=9 and +/+;Cre/+, n=11) were tested at 4 months of age.

Water Y-maze. Mice were tested in a Y-shaped maze (arms 34 cm long and 10 cm wide) filled with water (21°C) and a small amount of white paint. The submerged (1 cm) escape platform was located at one end of the arms of the maze. The location of the platform was alternated between cages. Mice were given 5 blocks of trials to learn the platform location. Each block consisted of 5 trials separated by approximately 30 sec – 2 min. Each block was separated by approximately 1 hr. 24 hours after the training, mice were given another 2 blocks of trials with the platform in the same location to assess whether they had learned the location. Mice that did not score 80% or better were excluded from analysis. 24 hrs. after the test the platform was moved to the arm opposite the location they were trained and the mice were given another 5 blocks of trials to learn this new location. Once the mouse entered an arm, the data were scored as either correct (the arm which contained the platform) or an error (the arm which did not contain the platform). CAG-FUS^{R521G} (Tg/+;Cre/+, n=18) and littermate controls (Tg/+;+/+, n=19 and +/+;Cre/+, n=19) were tested at 2 months of age.

Olfactory Discrimination Test. Mice were placed individually into a clean mouse cage with bedding and allowed to habituate for 15-45 min. During this time a dry, long-handled cotton-tipped applicator was placed through the lid into the center of the cage and lowered to the height of the mice. For the test, the cage was moved into a quiet, dimly lit room to minimize any anxiety. The applicator was replaced by new cotton tipped applicator that had been dipped into water. The time that the mouse sniffed this applicator during a 2 min period was recorded. This process was repeated a total of three times with a new applicator used for each test. The test was then repeated with an applicator which had been run through the dirty bedding of another mouse cage. This test was also repeated 3 times with a new applicator dipped into the dirty bedding. Sniffing was defined as the mouse's nose pointed in the direction of the applicator and within approximately 1 cm. CAG-FUS^{R521G} (Tg/+;Cre/+, n=18) and littermate controls (Tg/+;+/+, n=19 and +/+;Cre/+, n=19) were tested at 4 months of age.

All behaviour testing were performed on CAG-FUS^{WT}, CAG-FUS^{R521G} and their littermate controls. There were no sex differences observed for any behavioral tests performed and sexes were evenly distributed for each genotype tested.

Paired-end RNA-seq. Spinal cords were dissected from control and transgenic mice at postnatal day P20 and stored at -80°C until total RNA was extracted using RNA Stat 60 reagent (Amsbio). Selected mice were between a health score of 1-2 as described in the material and methods in the main text. The mice were carefully selected to be phenotypically similar. Additionally, each paired-end RNA-Seq library was generated using equal amounts of RNA pooled from 3 animals, to take into account phenotypic variability. Quality of RNA was assessed with a Bioanalyzer using a nanochip. RNA samples with RIN (RNA integrity number) > 7 were used for RNA-Seq and qRT-PCR. Paired-end RNA-Seq libraries were generated for CAG-FUS^{WT} (n=2), CAG-FUS^{R521G} (n=2) and their littermate controls (n=2) using the Illumina TruSeq RNA Sample Preparation Kit v2 (RS-122-2001). A total of ~630 million paired-end RNA-Seq reads (2 x 100nt) were obtained using the Illumina HiSeq GAII sequencing platform. Reads were mapped to reference mouse genome (mm10) using TopHat (8-

10) (v 2.0.4) with default parameters (read alignment with up to 2 mismatches allowed, using a known mouse reference annotation (UCSC genes), etc.). Post read-mapping DESeq (11) was implemented to identify the differentially expressed genes (DEG).

Properly paired mapped reads were used to identify differentially expressed genes using read DESeq (11). DESeq (11) is an R/Bioconductor package based method which employs a negative binomial distribution method to quantify differential gene expression between transgenic samples and control samples, using count data from mapped RNA-Seq reads. HTSeq (12) (a python based tool) was used to generate the count data for each condition. DESeq (11) identified differentially expressed genes (with adjusted P-value < 0.05) which were assessed for functional annotation using the DAVID (13) functional annotation tool.

Statistical Analysis. Results are expressed as the mean ± SEM (standard error of the mean) or ± SD (standard deviation) where indicated. Three-way statistical comparisons use one-way ANOVA (GraphPad Prism version 6). We utilized a two-tailed, unpaired Student's t-test for all pair-wise comparisons (GraphPad Prism version 6). *P* values less than 0.05 were considered significant.

Genotyping. Genomic DNA from ear biopsies were lysed in Quick Lysis Buffer (50 mM NaCl, 10 mM Tris-HCl pH 8.3, 0.2% Tween 20 and 0.4 mg/ml proteinase K) at 55ºC for 1 hour and then 95ºC for 10 min. The PCR contained genomic DNA, genotyping primers (listed below) and standard Taq buffer supplemented with 1 M betaine, 3.3% DMSO (vol/vol), 1.5 mM $MgCl_2$, 0.1 mg/ml BSA, 0.2 mM deoxynucleoside triphosphates and 1.25 units of *Taq* polymerase (New England Biolabs, NEB). After enzymatic amplification for 35 cycles, the PCR products were resolved on 2% agarose gel (wt/vol) in 1X Tris acetate-EDTA buffer.

Genotyping Primers:

Gene symbol	Forward primer	Reverse primer
Cre	GCATAACCAGTGAAACAGCATTGC	GGACATGTTCAGGGATCGCCAGGC
GFP	CTGACCCTGAAGTTCATCTGCACC	TGGCTGTTGTAGTTGTACTCCAGC
Human FUS	GACCAGGTGGCTCTCACATG	GTCGCTACAGACGTTGTTTGTC
Internal control (Pin1)	ATCATCCTGCGCACAGAATG	TCAATTCCTCCAGAAGGAGC

SUPPLEMENTAL FIGURE LEGENDS

Figure S1. (A,B) Genotyping results from Meox2Cre crosses from three founders from the *CAG-Z-FUS^{WT}-EGFP* (lines: 629 and 638) and *CAG-Z-FUS^{R521G}-EGFP* (lines: 673 and 682) transgenic lines. PCR products using primers for FUS, GFP, Cre and Pin1 (internal control) are shown. (C) FISH (fluorescent in situ hybridization) of chromosomes isolated from CAG-FUS^{WT} (629) and CAG-FUS^{R521G} (673) MEF cells. CAG-FUS^{WT} (629) and CAG-FUS^{R521G} (673) founders show single insertion of transgenes. (D) Immunoblot of HeLa total cell lysates (human) and whole mouse brain lysates (mouse) showing molecular weight differences for human and mouse FUS protein. (E,F) Immunostaining for GFP (green) shows specific staining in brain and spinal cord of CAG-FUS^{WT} and CAG-FUS^{R521G} mice (P0) and increased staining for FUS (red, Sigma,

HPA008784). Spinal cord sections from end-stage CAG-FUS^{WT} and CAG-FUS^{R521G} mice are co-stained with (G) anti-hFUS (red) and anti-GFP (green) or (H) Ubiquitin (red) and FUS (green, Santa Cruz). No mislocalization or ubiquitination of human FUS^{WT} or FUS^{R521G} are observed. (G,H) Shown is the ventral horn of the lumbar region of the spinal cord.

Figure S2. (A-B) Body weights of CAG-FUS^{WT} (638) and CAG-FUS^{R521G} (682) mice from P0-P20. (C-D) Body weights of female and male CAG-FUS^{R521G} (682) mice from 5-14 weeks of age. (E) Grip test of CAG-FUS^{R521G} (682) mice, postnatal stages (P14-30), n=17 litters. Red circles (**o**) indicate CAG-FUS^{R521G} mice that had loss of motor function and early lethality. (A-E) Error bars represent SD of the mean.

Figure S3. ImageJ quantification of integrated density of GFAP and Iba1 staining in (A) CAG-FUS^{WT} and (B) CAG-FUS^{R521G} mice. Immunofluorescence staining of CAG-FUS^{R521G} mice that escape early lethality in the CA3 region of the hippocampus (C) and of the ventral horn of the spinal cord (D) for Iba1 (microglia;red) and GFAP (astrocytes;green) showing no neuroinflammation. (A,B) Quantification of microglia and astrocytes a, $P < 0.05$; b, $P < 0.01$; c. $P < 0.005$ (Student *t* test). Error bars represent SEM of the mean.

Figure S4. H&E staining of the hippocampus and cortex (A) showing no loss of cells. Toluidine blue staining of dorsal and ventral roots (L4-5) (B), dorsal cortical (DCST) and lateral spinal tracts (LST) (C) of CAG-FUS^{WT} and CAG-FUS^{R521G} mice (P20-23) showing no changes in myelinated axons. (D) Cresyl violet (top panel) and H&E (bottom panel) staining of cervical spinal cord from aged CAG-FUS^{R521G} mice (2 years old). (E) Quantification of cervical motor neurons from CAG-FUS^{R521G} mice (2 years old). Student *t* test shows no significant differences between groups. ns, not significant. Error bars represent SEM of the mean.

Figure S5. (A) Neuromuscular junctions (NMJ) from CAG-FUS^{WT} and CAG-FUS^{R521G} mice at end-stage are costained for presynaptic terminals (nerve;red) and bungarotoxin for postsynaptic terminals (AchR;green) showing abnormal morphology compared with littermate controls. (B,C) NMJs in CAG-FUS^{WT} and CAG-FUS^{R521G} mice (P20) stain positive for terminal myelinating Schwann cells (S100B;red), GFP;green, and bungarotoxin for postsynaptic terminals (AchR;blue), although their morphology is not typical of the pretzel shape observed in control (CTL) mice.

Figure S6. MA plot showing differentially expressed genes (DEG) in (A) CAG-FUS^{WT} (638) transgenic mice against control wild-type mice, and (B) CAG-FUS^{R521G} (682) transgenic mice against control wild-type mice. All genes are shown in grey and DEG are shown in black. CAG-FUS^{WT} transgenic mice show more genes affected compared to CAG-FUS^{R521G}.

Figure S7. (A) Open field test from 2 and 4 month old CAG-FUS^{R521G} mice and littermates show no differences in total distance travelled. (B) Total daily food intake and (C) food intake per body weight of 2 month old CAG-FUS^{R521G} (682) mice during running wheel testing. (D) Digigait trace for a control animal showing parameters that are measured for gait analysis. Ladder walking test shows the forepaws have a lower step score (E) and more errors per step (F). Hindpaws show no deficits (G,H). Social interactions of CAG-FUS^{R521G} mice were

reduced with juveniles at 2 months and significantly decreased by 4 months of age (I). All mice performed equally in a Y-test which measures learning and decision making (J). Shown are the results from reversal testing that measures the ability of the mice to find the platform in the opposite arm to which they were entrained (J). Olfaction testing showing no alterations in CAG-FUS^{R521G} mice (K). Studies were conducted with littermate controls (+/+;Cre/+ and Tg/+;+/+), which showed no statistical impairments. (A,E-K) Statistical comparisons uses one-way ANOVA. a, $P < 0.05$; b, $P < 0.01$. (‘ compares +/+;Cre/+ with Tg/+;Cre/+). (B,C) Uses Student *t* test. ns, not significant. Error bars represent SEM of the mean.

Figure S8. Li-Cor Odyssey quantification for synaptic proteins Arc, CamKII, GluR1 and Psd-95 from (A,C) total cell lysates (TCL) and (B,D) synaptoneurosomes (SN). The graphs represent the average of 3-5 independent experiments. Student’s *t* test shows no statistical differences in protein expression between CAG-FUS^{WT} and CAG-FUS^{R521G} (682) compared to their littermate controls (CTL). Error bars represent SEM of the mean.

Movie S1. Video recording of a control resident mouse from the 8-month resident-intruder test. The video clip is representative of the mean interaction of the control groups. The control resident “test” mouse (#3935) shows normal social behaviors towards the “novel” intruder mouse. The video shown is taken 4 min after the intruder mouse is introduced into the home cage.

Movie S2. Video recording of a CAG-FUS^{R521G} resident mouse from the 8-month resident-intruder test. The video clip is representative of the mean interaction of the CAG-FUS^{R521G} group. The CAG-FUS^{R521G} resident “test” mouse (#3890) spends less time chasing the “novel” intruder mouse and displays less active social behavior overall. The video shown is taken 4 min after the intruder mouse is introduced into the home cage.

REFERENCES

1. Huang C*, et al.* (2011) FUS transgenic rats develop the phenotypes of amyotrophic lateral sclerosis and frontotemporal lobar degeneration. *PLoS Genet* 7(3):e1002011.
2. Sephton CF*, et al.* (2010) TDP-43 is a developmentally regulated protein essential for early embryonic development. *J Biol Chem* 285(9):6826-6834.
3. Qiu H*, et al.* (2014) ALS-associated mutation FUS-R521C causes DNA damage and RNA splicing defects. *The Journal of clinical investigation* 124(3):981-999.
4. Tsai NP*, et al.* (2012) Multiple autism-linked genes mediate synapse elimination via proteasomal degradation of a synaptic scaffold PSD-95. *Cell* 151(7):1581-1594.
5. Sephton CF*, et al.* (2011) Identification of neuronal RNA targets of TDP-43-containing ribonucleoprotein complexes. *J Biol Chem* 286(2):1204-1215.
6. Farr TD, Liu L, Colwell KL, Whishaw IQ, & Metz GA (2006) Bilateral alteration in stepping pattern after unilateral motor cortex injury: a new test strategy for analysis of skilled limb movements in neurological mouse models. *Journal of neuroscience methods* 153(1):104-113.
7. Tennant KA & Jones TA (2009) Sensorimotor behavioral effects of endothelin-1 induced small cortical infarcts in C57BL/6 mice. *Journal of neuroscience methods* 181(1):18-26.
8. Trapnell C, Pachter L, & Salzberg SL (2009) TopHat: discovering splice junctions with RNA-Seq. *Bioinformatics* 25(9):1105-1111.
9. Kim D*, et al.* (2013) TopHat2: accurate alignment of transcriptomes in the presence of insertions, deletions and gene fusions. *Genome biology* 14(4):R36.

10. Langmead B, Trapnell C, Pop M, & Salzberg SL (2009) Ultrafast and memory-efficient alignment of short DNA sequences to the human genome. *Genome biology* 10(3):R25.
11. Anders S & Huber W (2010) Differential expression analysis for sequence count data. *Genome biology* 11(10):R106.
12. Narayanan U*, et al.* (2007) FMRP phosphorylation reveals an immediate-early signaling pathway triggered by group I mGluR and mediated by PP2A. *The Journal of neuroscience : the official journal of the Society for Neuroscience* 27(52):14349-14357.
13. Huang da W, Sherman BT, & Lempicki RA (2009) Systematic and integrative analysis of large gene lists using DAVID bioinformatics resources. *Nature protocols* 4(1):44-57.

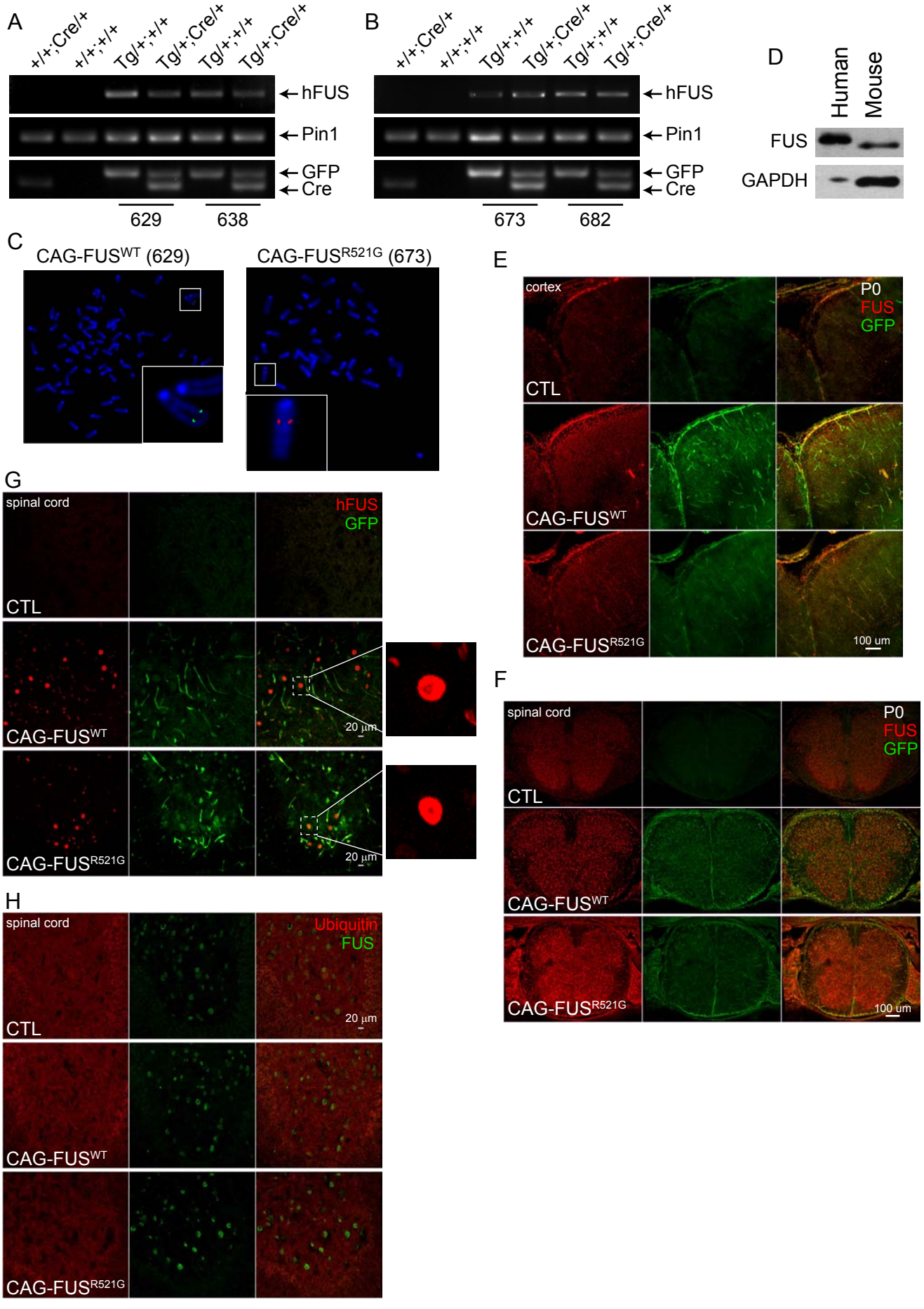
A
+/+;Cre/+
+/+;+/+
Tg/+;+/+
Tg/+;Cre/+
Tg/+;+/+
Tg/+;Cre/+
hFUS
Pin1
GFP
Cre
629
638
B
673
682
D
Human
Mouse
FUS
GAPDH
C
CAG-FUSWT (629)
CAG-FUSR521G (673)
E
cortex
P0
FUS
GFP
CTL
CAG-FUSWT
CAG-FUSR521G
100 um
F
spinal cord
G
hFUS
20 μm
H
Ubiquitin

Figure S1

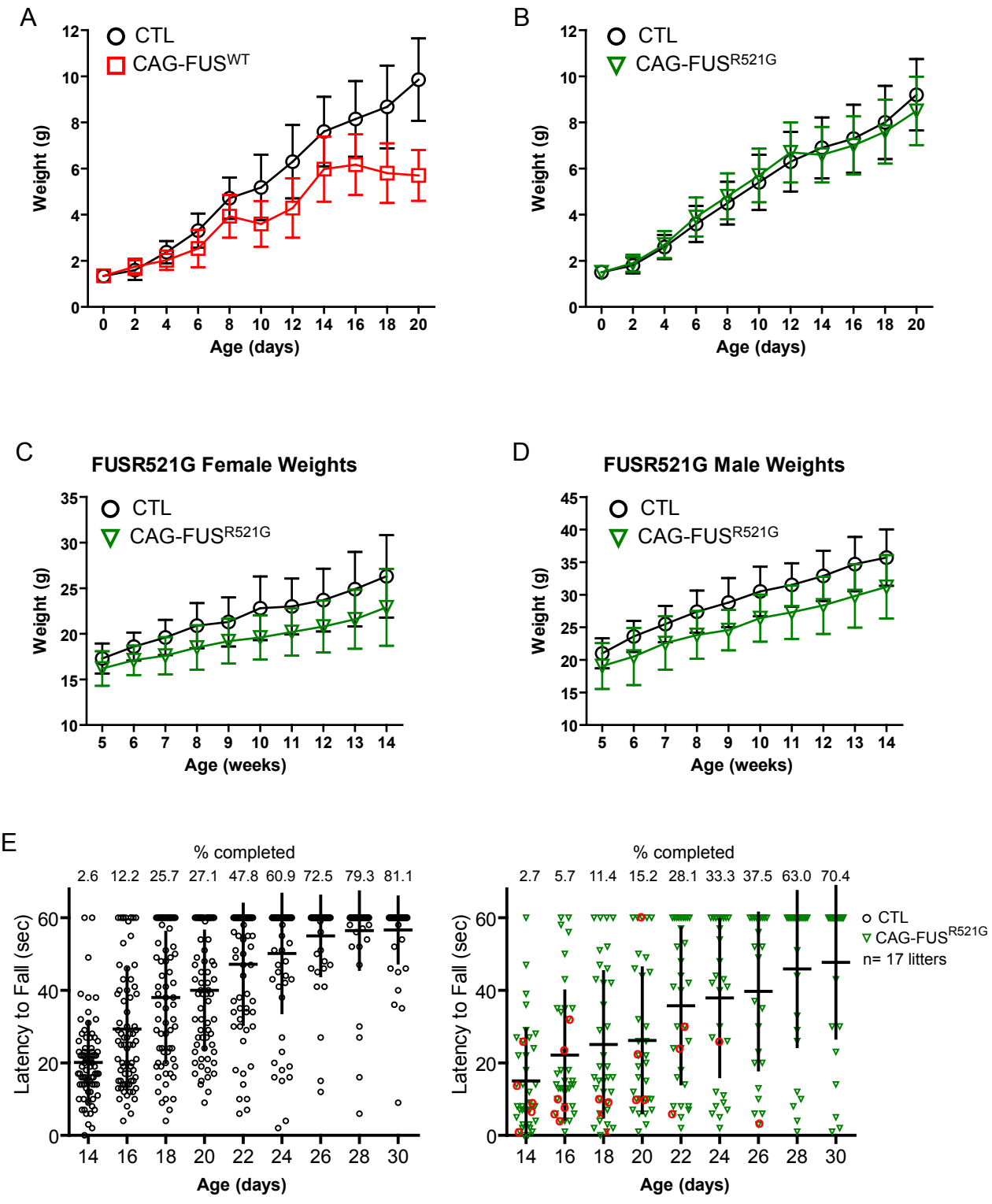
A
CTL
CAG-FUSWT
Weight (g)
Age (days)
B
CTL
CAG-FUSR521G
Weight (g)
Age (days)
C
FUSR521G Female Weights
CTL
CAG-FUSR521G
Weight (g)
Age (weeks)
D
FUSR521G Male Weights
CTL
CAG-FUSR521G
Weight (g)
Age (weeks)
E
% completed
2.6 12.2 25.7 27.1 47.8 60.9 72.5 79.3 81.1
Latency to Fall (sec)
Age (days)
% completed
2.7 5.7 11.4 15.2 28.1 33.3 37.5 63.0 70.4
Latency to Fall (sec)
Age (days)
CTL
CAG-FUSR521G
n= 17 litters

Figure S2

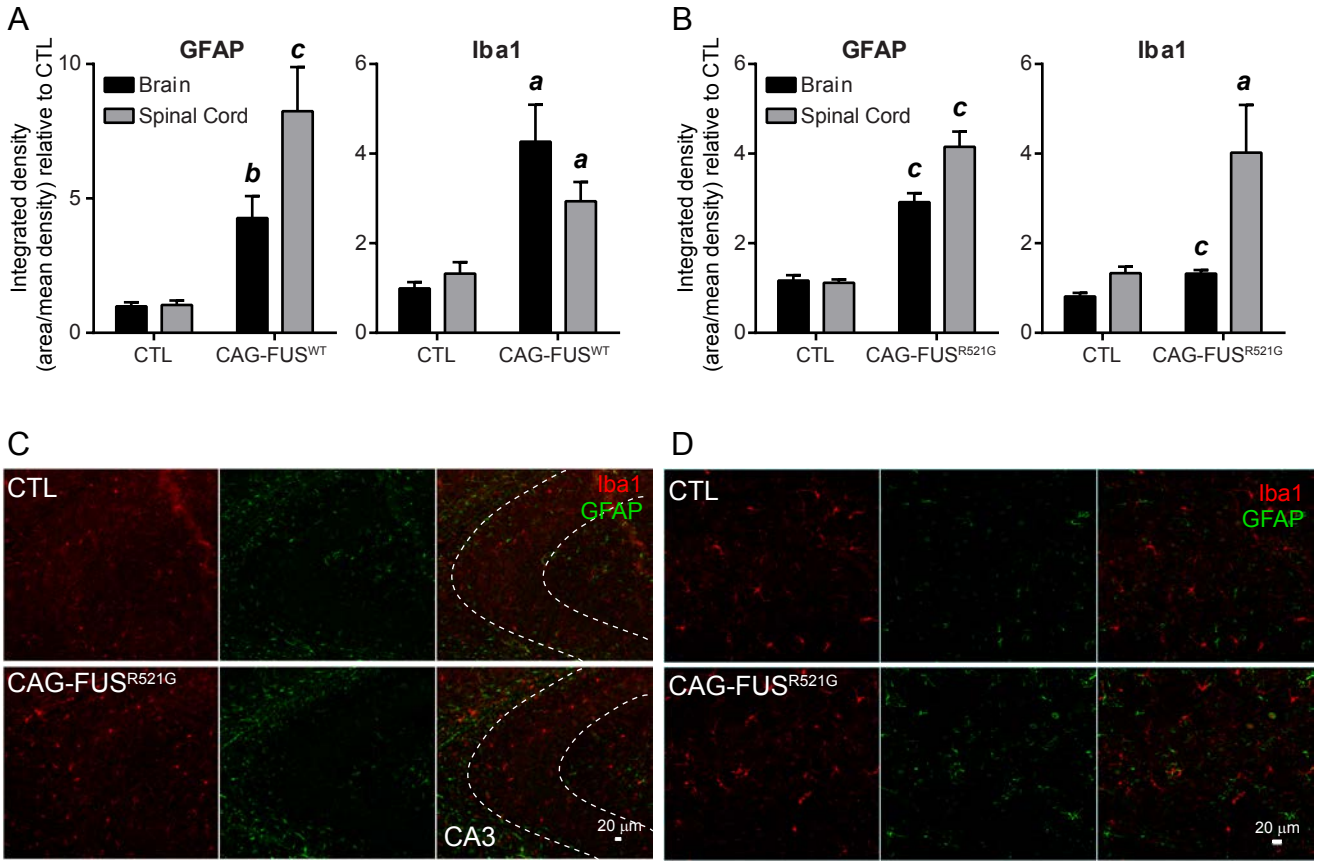
A
GFAP
Iba1
Brain
Spinal Cord
Integrated density (area/mean density) relative to CTL
CTL
CAG-FUSWT
B
CAG-FUSR521G
C
D
Iba1
GFAP
CA3
20 µm

Figure S3

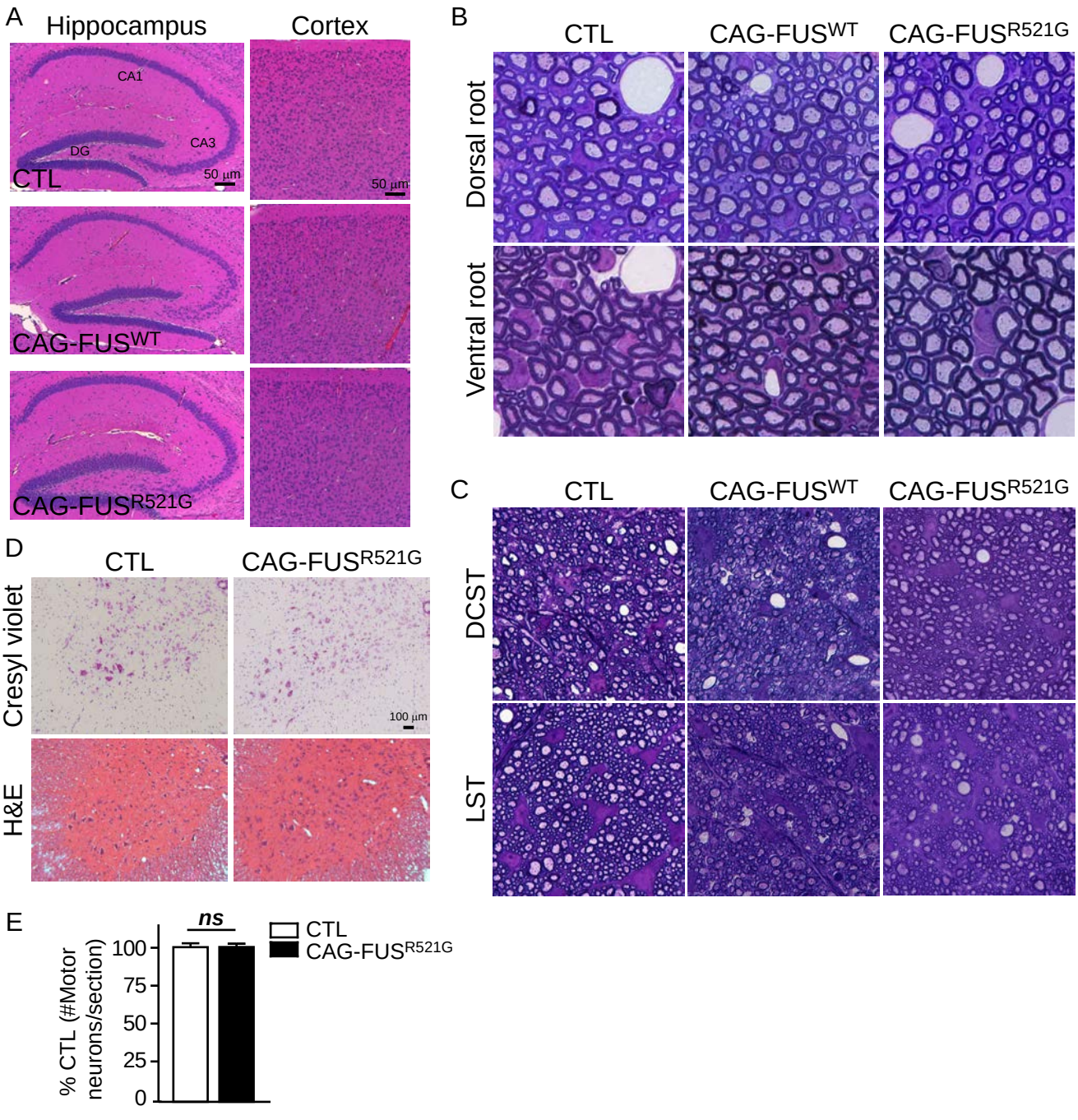
A
Hippocampus
Cortex
CA1
DG
CA3
CTL
50 μm
50 μm
CAG-FUSWT
CAG-FUSR521G
B
CTL
CAG-FUSWT
CAG-FUSR521G
Dorsal root
Ventral root
C
CTL
CAG-FUSWT
CAG-FUSR521G
DCST
LST
D
CTL
CAG-FUSR521G
Cresyl violet
H&E
100 μm
E
ns
CTL
CAG-FUSR521G
% CTL (#Motor neurons/section)
100
75
50
25
0

Figure S4

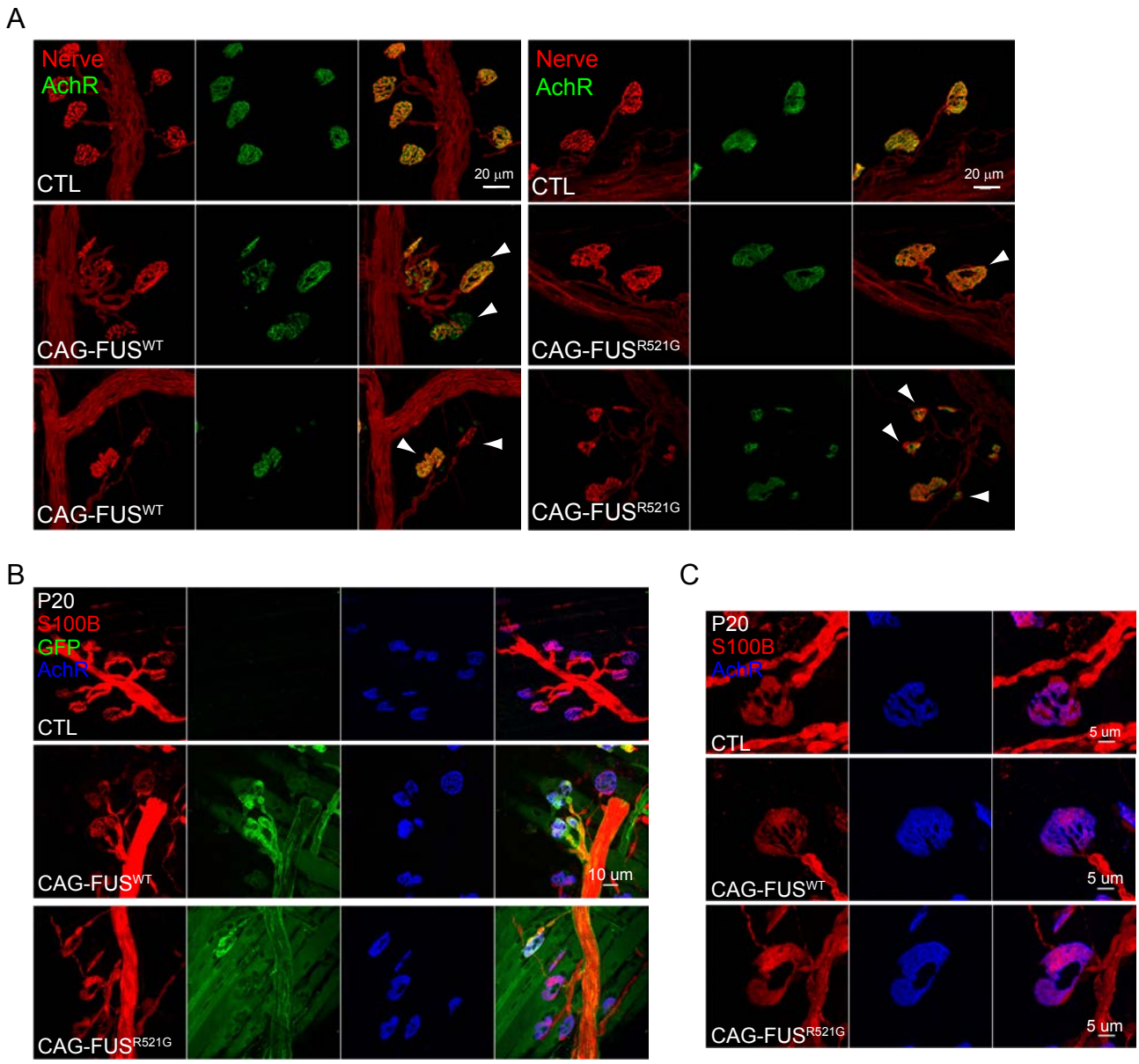
A
Nerve
AchR
CTL
20 μm
Nerve
AchR
CTL
20 μm
CAG-FUSWT
CAG-FUSR521G
CAG-FUSWT
CAG-FUSR521G
B
P20
S100B
GFP
AchR
CTL
CAG-FUSWT
10 um
CAG-FUSR521G
C
P20
S100B
AchR
CTL
5 um
CAG-FUSWT
5 um
CAG-FUSR521G
5 um

Figure S5

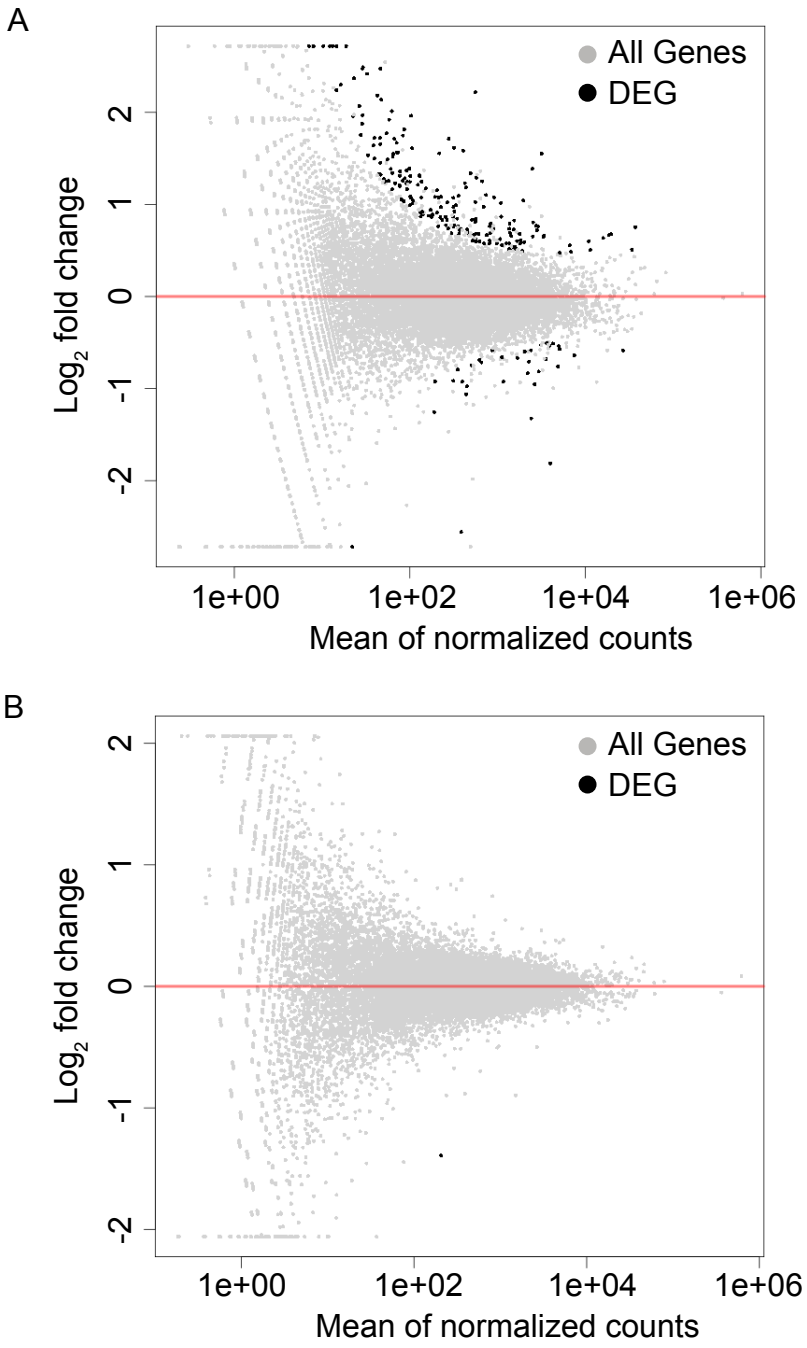
A
All Genes
DEG
Log2 fold change
2
1
0
-1
-2
1e+00
1e+02
1e+04
1e+06
Mean of normalized counts
B
All Genes
DEG
Log2 fold change
2
1
0
-1
-2
1e+00
1e+02
1e+04
1e+06
Mean of normalized counts

Figure S6

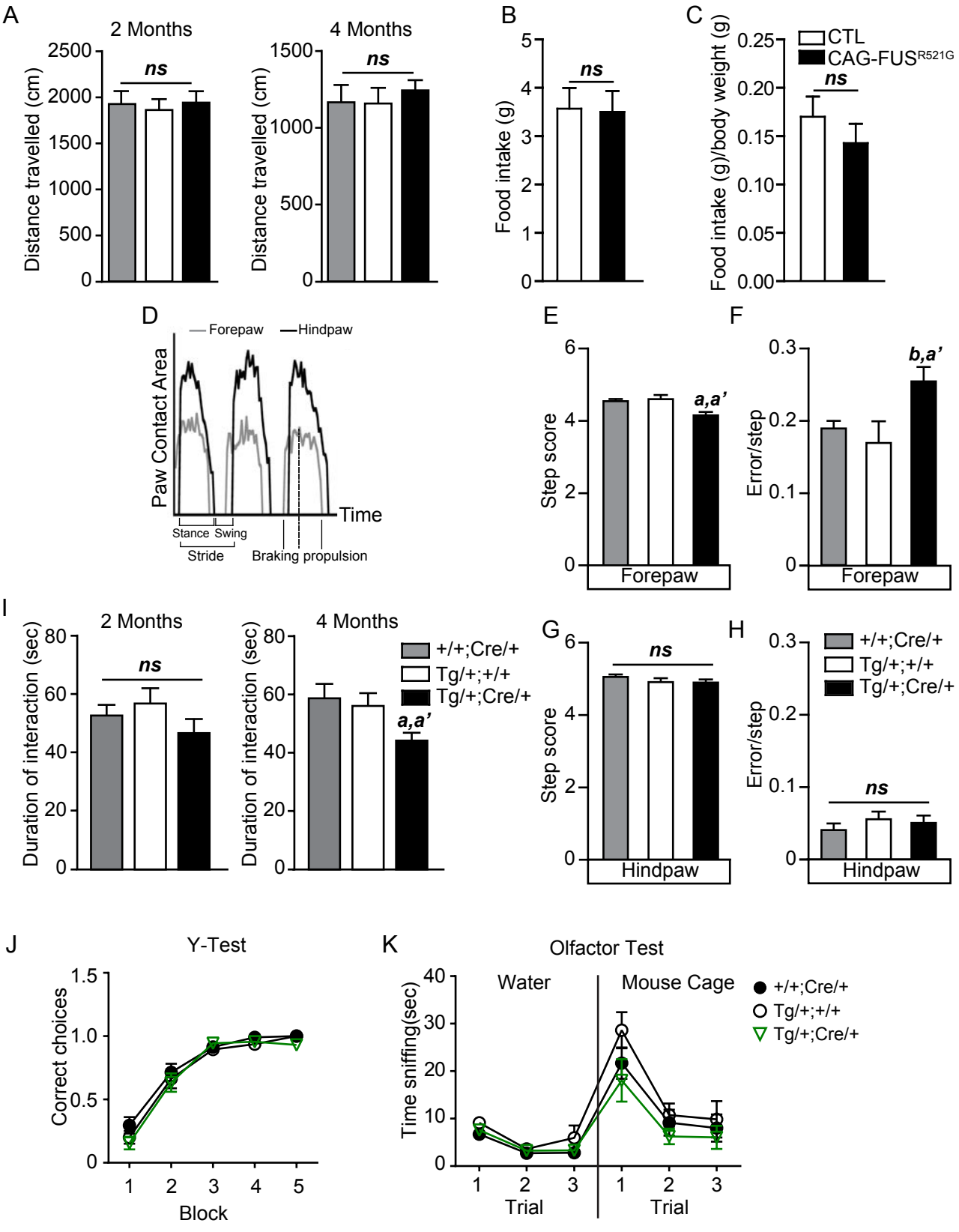
A
2 Months
4 Months
Distance travelled (cm)
ns
B
Food intake (g)
C
Food intake (g)/body weight (g)
CTL
CAG-FUS R521G
D
Forepaw
Hindpaw
Paw Contact Area
Time
Stance
Swing
Stride
Braking propulsion
E
Step score
a,a'
Forepaw
F
Error/step
b,a'
G
Hindpaw
H
I
Duration of interaction (sec)
+/+;Cre/+
Tg/+;+/+
Tg/+;Cre/+
J
Y-Test
Correct choices
Block
K
Olfactor Test
Water
Mouse Cage
Time sniffing(sec)
Trial

Figure S7

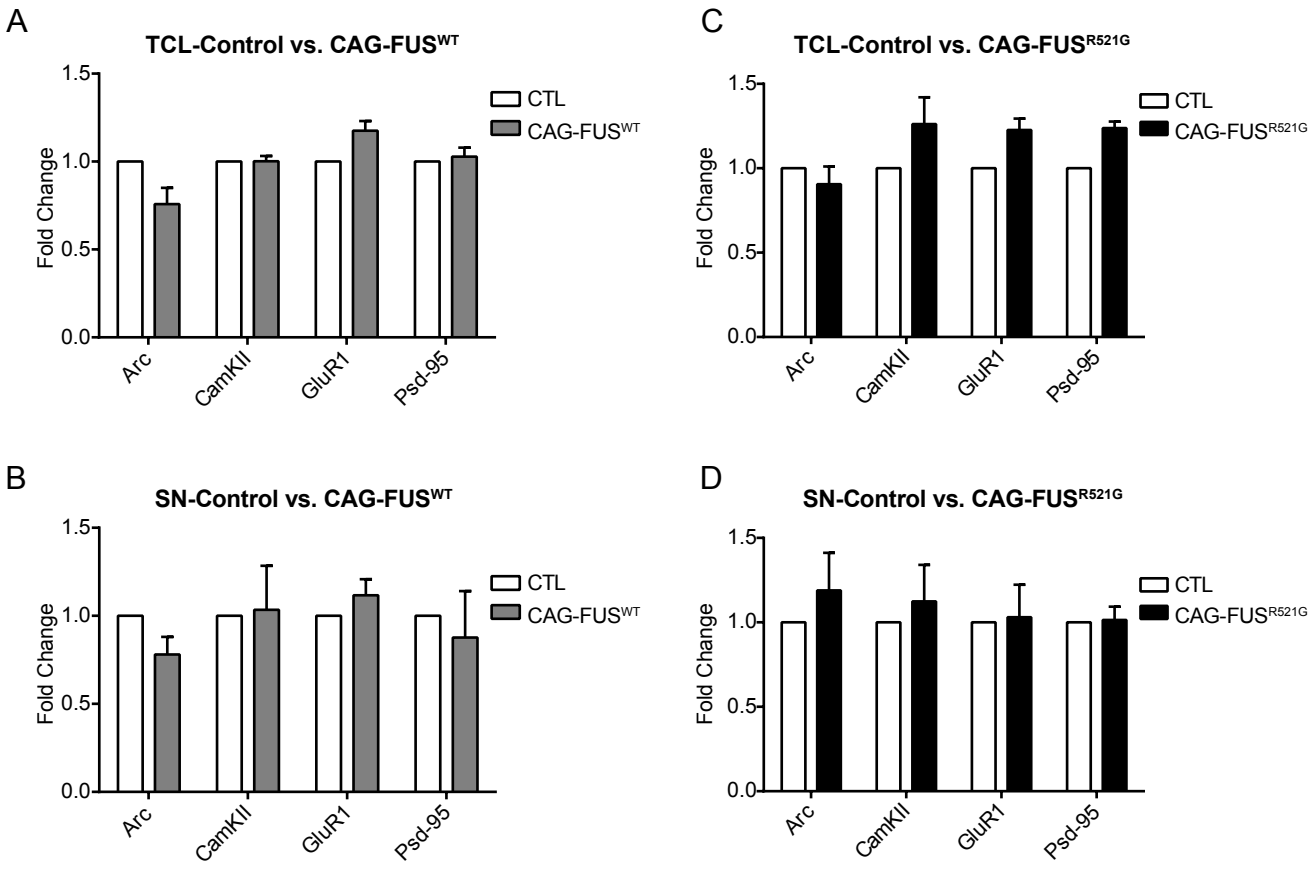
A
TCL-Control vs. CAG-FUSWT
Fold Change
1.5
1.0
0.5
0.0
CTL
CAG-FUSWT
Arc
CamKII
GluR1
Psd-95
C
TCL-Control vs. CAG-FUSR521G
Fold Change
1.5
1.0
0.5
0.0
CTL
CAG-FUSR521G
Arc
CamKII
GluR1
Psd-95
B
SN-Control vs. CAG-FUSWT
Fold Change
1.5
1.0
0.5
0.0
CTL
CAG-FUSWT
Arc
CamKII
GluR1
Psd-95
D
SN-Control vs. CAG-FUSR521G
Fold Change
1.5
1.0
0.5
0.0
CTL
CAG-FUSR521G
Arc
CamKII
GluR1
Psd-95

Figure S8

Table S1. Genotypes of P0 offspring from Tg/+;+/+ x Meox2Cre intercrosses

CAG-FUS^{WT}					
Line:	**+/+;Cre/+**	**+/+;+/+**	**Tg/+;+/+**	**Tg/+;Cre/+**	**Total**
629	24%	24%	25%	26%	95
638	23%	22%	21%	34%	120
CAG-FUS^{R521G}					
Line:	**+/+;Cre/+**	**+/+;+/+**	**Tg/+;+/+**	**Tg/+;Cre/+**	**Total**
673	24%	25%	22%	28%	99
682	27%	17%	29%	26%	66
Expected ratio:	25%	25%	25%	25%	

Table S2. Grip test of CAG-FUS^{WT} and CAG-FUS^{R521G} mice

Age (days)	CTL		CAG-FUS^{WT}	
	Mean (sec)	% Complete	Mean (sec)	% Complete
14	24.9 ± 4.0	3.1	3.8 ± 1.1 ***d***	0.0
16	39.2 ± 4.6	28.8	1.6 ± 0.5 ***d***	0.0
18	45.8 ± 4.0	47.9	0.6 ± 0.2 ***d***	0.0
20	50.8 ± 3.6	61.5	0.4 ± 0.2 ***d***	0.0

Age (days)	CTL		CAG-FUS^{R521G}	
	Mean (sec)	% Complete	Mean (sec)	% Complete
14	20.1 ± 2.7	2.6	15.1 ± 3.3	2.9
18	38.0 ± 4.2	25.7	27.4 ± 4.6 ***b***	12.9
22	47.2 ± 3.5	47.8	37.4 ± 4.6 ***a***	31.0
26	55.0 ± 2.2	72.5	41.3 ± 4.1 ***d***	39.1
30	56.6 ± 1.7	81.1	47.7 ± 3.9 ***b***	70.4

Student's *t*-test, ***a***,p<0.05; ***b***,p<0.01; ***d***,p<0.001
± SE (standard error of mean)

Table S3. Paired-end RNA-Seq reads summary

Samples	Properly paired reads	Quality passed reads	Total reads
FUS WT CTL1	55803368	74643906	85838586
FUS WT CTL2	28519390	37892168	86599378
FUS WT TG1	45656532	60879824	79388726
FUS WT TG2	67191840	90452989	67018964
FUS R521G CTL1	55028504	74358495	89150552
FUS R521G CTL2	57491368	75476514	44661408
FUS R521G TG1	52537060	68914387	72153918
FUS R521G TG2	42963068	58682073	106147744

Note: For two samples, the number of properly paired reads/quality passed reads is larger than total reads for those samples. This is due to the fact that Tophat allows reads to map to more than one place in the genome (multihits) as its default parameter, which causes such reads to be counted more than once, leading to increased number of reads in the BAM file after mapping compared to total reads in the FASTQ file.

Table S4. Forepaw gait measurements of CAG-FUS^{R521G} mice

	+/+;Cre/+ (n=19)	**Tg/+;+/+ (n=19)**	**Tg/+;Cre/+ (n=18)**
Paramenter	Mean	Mean	Mean
Swing Stride (%)	38.4 ± 0.5	38.9 ± 0.5	37.5 ± 0.7
Brake Stride (%)	30.1 ± 1.4	29.3 ± 1.5	34.8 ± 1.2 ***a,b'***
Propel Stride (%)	31.4 ± 1.5	31.8 ± 1.6	27.7 ± 1.4
Brake Stance (%)	49.1 ± 2.3	48.1 ± 2.6	55.8 ± 2.1 ***b,ns'***
Propel Stance (%)	50.9 ± 2.3	51.9 ± 2.6	44.2 ± 2.1
Stride Length (cm)	5.72 ± 0.10	5.82 ± 0.05	5.65 ± 0.08
Stance Width (cm)	1.46 ± 0.05	1.51 ± 0.05	1.46 ± 0.05
Midline Distance (cm)	-2.08 ± 0.09	-2.20 ± 0.09	-2.17 ± 0.09

One-way ANOVA, a,$p<0.05$; b,$p<0.01$; ns,not significant, ' compares +/+;Cre/+ with Tg/+;Cre/+
± SE (standard error of mean)

Table S5. Hindpaw gait measurements of CAG-FUS^{R521G} mice

	+/+;Cre/+ (n=19)	**Tg/+;+/+ (n=19)**	**Tg/+;Cre/+ (n=18)**
Paramenter	Mean	Mean	Mean
Swing Stride (%)	35.4 ± 0.6	34.9 ± 0.5	32.8 ± 0.8 ***a,b'***
Brake Stride (%)	18.1 ± 0.8	18.8 ± 0.8	17.8 ± 0.8
Propel Stride (%)	46.4 ± 0.8	46.3 ± 0.8	49.4 ± 1.2
Brake Stance (%)	28.0 ± 1.2	28.1 ± 1.1	26.6 ± 1.3
Propel Stance (%)	72.0 ± 1.2	71.2 ± 1.1	73.4 ± 1.3
Stride Length (cm)	5.74 ± 0.10	5.86 ± 0.06	5.73 ± 0.09
Stance Width (cm)	2.66 ± 0.05	2.55 ± 0.06	2.62 ± 0.05
Midline Distance (cm)	1.62 ± 0.04	1.61 ± 0.06	1.42 ± 0.07 ***a,a'***

One-way ANOVA, a,p<0.05; b,p<0.01, ' compares +/+;Cre/+ with Tg/+;Cre/+
± SE (standard error of mean)

Supporting Information

Sephton et al. 10.1073/pnas.1406162111

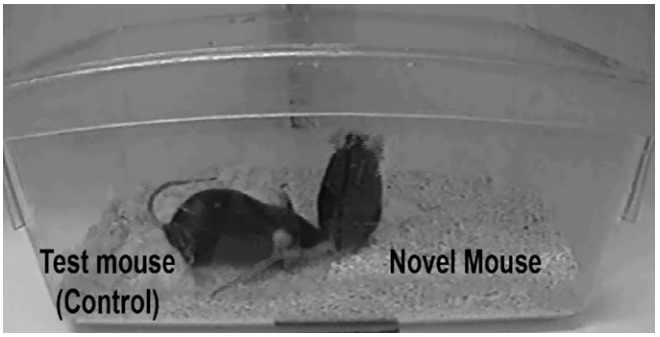

Movie S1. Video recording of a control resident mouse from the 8-month resident-intruder test. The video clip is representative of the mean interaction of the control groups. The control resident "test" mouse (#3935) shows normal social behaviors towards the "novel" intruder mouse. The video shown is taken 4 min after the intruder mouse is introduced into the home cage.

Movie S1

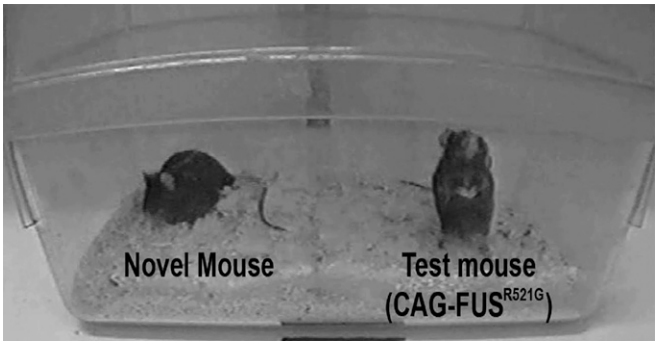

Movie S2. Video recording of a CAG-FUS^{R521G} resident mouse from the 8-month resident-intruder test. The video clip is representative of the mean interaction of the CAG-FUS$_{R521G}$ group. The CAG-FUS^{R521G} resident "test" mouse (#3890) spends less time chasing the "novel" intruder mouse and displays less active social behavior overall. The video shown is taken 4 min after the intruder mouse is introduced into the home.

Movie S2

Other Supporting Information Files

SI Appendix (PDF)